

This document is not an API Standard; it is under consideration within an API technical committee but has not received all approvals required to become an API Standard. It shall not be reproduced or circulated or quoted, in whole or in part, outside of API committee activities except with the approval of the Chairman of the committee having jurisdiction and staff of the API Standards Dept. Copyright API. All rights reserved.

Evaluating Metallic Material Performance in High-Pressure Hydrogen Gas

API TECHNICAL REPORT 21C

FIRST EDITION, XXXXXXXXXXXX 202X

Comment Only Ballot - For Committee Review

This document is not an API Standard; it is under consideration within an API technical committee but has not received all approvals required to become an API Standard. It shall not be reproduced or circulated or quoted, in whole or in part, outside of API committee activities except with the approval of the Chairman of the committee having jurisdiction and staff of the API Standards Dept. Copyright API. All rights reserved.

Table of Contents

1	Scope	3
2	Normative References	3
3	Abbreviations and Variables	3
4	Background	4
4.1	General	4
4.2	Test Program	4
4.2.1	Materials	5
4.2.2	Test Environment	6
4.2.3	Test Methods	6
5	Summary of Testing Program Results	7
5.1	General	7
5.2	SSR Results	7
5.3	FT Results	15
5.3.1	4140-110 results	15
5.3.2	Alloy 718-120 results	17
5.4	Hydrogen Permeation Results	20
5.4.1	41XX-110	20
5.4.2	Alloy 718-120	22
6	Discussion	23
6.1	General	23
6.2	Comparison of Materials	23
6.3	Influence of Loading Parameters	25
	Bibliography	27
	A.1 TEST MATERIALS AND SPECIMENS	29
	A.1.1 Materials	29
	A.1.2 Specimen Description	29
	A.1.2.1 Slow Strain Rate (SSR) Specimen	29
	A.1.2.2 Fracture Toughness (FT) Specimen	30
	A.1.2.3 Hydrogen Permeation Specimen	31
	A.2 Test Matrix	32
	A.3 Test Details	33
	A.3.1 Environmental Testing procedure	33
	A.3.2 SSR Testing	33
	A.3.3 FT Testing	33
	A.3.4 Hydrogen Flux Measurement	35
	A.4 Data Analysis	36
	A.4.1 SSR Data Analysis	36
	A.4.2 FT Data Analysis	36
	A.4.3 Hydrogen Flux Data Analysis	37
	B.1 MATERIALS AND SPECIMEN GEOMETRIES	38

This document is not an API Standard; it is under consideration within an API technical committee but has not received all approvals required to become an API Standard. It shall not be reproduced or circulated or quoted, in whole or in part, outside of API committee activities except with the approval of the Chairman of the committee having jurisdiction and staff of the API Standards Dept. Copyright API. All rights reserved.

B.2 TEST METHODS 41
B.2.1 SSR Testing 41
B.2.2 FT Testing 41

1 Scope

Understanding the fracture behavior of metallic materials in high pressure H₂ environment can be useful for selection of materials in underground H₂ storage. Currently, there is sparse data on fracture mechanics of metallic materials typically used in oil and gas well construction when subject to high pressure H₂ gas environment. This test program is an effort to generating data to provide some insight into testing procedures, material behavior which over time could help the industry in evaluation and selection of materials in such service.

2 Normative References

There are no normative references in the document.

3 Abbreviations and Variables

3.1 Abbreviations and Variables

ϵ_p	plastic strain
ΔK	stress intensity factor range
K _{th}	threshold fracture toughness
FCGR	fatigue crack growth rate
FT	fracture toughness
PH	precipitation hardened
RA	reduction in area
RT	room temperature
SCE	saturated calomel electrode
SCGR	static crack growth rate
SSR	slow strain rate

This document is not an API Standard; it is under consideration within an API technical committee but has not received all approvals required to become an API Standard. It shall not be reproduced or circulated or quoted, in whole or in part, outside of API committee activities except with the approval of the Chairman of the committee having jurisdiction and staff of the API Standards Dept. Copyright API. All rights reserved.

SWCP seawater under cathodic potential

TTF time to failure

UTS ultimate tensile strength

WOL wedge opening loading

4 Background

4.1 General

Achieving net-zero carbon emissions by mid-century will require a transformation of the power and energy infrastructure, including the transition to hydrogen as a fuel of the future. While it is anticipated that hydrogen in near-term will be used in primarily smaller scale applications such as portable power, public transportation vehicles, and space applications, it is foreseeable that the future use of hydrogen would include use in industries such as steel, cement, shipping and other transportation etc. This setup will require an infrastructure that can deliver hydrogen from its source to the end users in large volumes. Therefore, providing hydrogen storage, transmission and delivery infrastructure will be critical for such applications. Currently there are ongoing efforts in the industry to understand and overcome challenges than can be presented for use of hydrogen.

In addition to using pipeline network for hydrogen transmission, large scale storage options beyond surface storage tanks or cryogenic vessels are needed. Underground storage wells have been successfully used for storing large volumes of natural gas (methane) for many decades now to facilitate use of it in power generation, feedstock for chemical plants on demand. Similar approach with hydrogen could provide a low or no carbon fuel for these applications. Geological formations such as salt caverns, depleted wells, mines, aquifers, hard rock caverns and mine seams can provide a means to store large volumes of hydrogen and thus, would have significant impact in providing the required energy in a hydrogen-based economy. The benefits and drawbacks of each of the above listed geological formations for hydrogen storage have been extensively reviewed [1-5]. Despite some similarities between storage of natural gas and hydrogen gas; underground well storage of hydrogen can be more complex due to physical, chemical properties differences between the two cases. Some of the differences such as the smaller size of hydrogen molecule and lower viscosity can lead to leaks; chemical reactions during storage could lead to production of other corrosive elements such as H₂S, acids etc. All these could factor in material choice for such applications.

For use of metallic materials in underground storage wells concerns of Hydrogen Embrittlement (HE) from exposure to high-pressure hydrogen gas needs to be addressed. Embrittlement can cause sudden, catastrophic failure of equipment hence understanding the HE susceptibility of various metals that could be used for underground hydrogen storage would be very important for optimum material selection. In this testing program the main objective was to evaluate test methods that can be used for understanding HE resistance in high pressure hydrogen gas and also provide comparison of performance of metallic materials typically used for underground storage well construction.

4.2 Test Program

This was the first metallic material test program initiated by the work group and was designed based on consensus opinion within the work group. This was based on typical conditions that could be applicable to underground hydrogen storage wells, test methods that could be suitable for evaluation and capability of multiple labs to conduct testing.

This document is not an API Standard; it is under consideration within an API technical committee but has not received all approvals required to become an API Standard. It shall not be reproduced or circulated or quoted, in whole or in part, outside of API committee activities except with the approval of the Chairman of the committee having jurisdiction and staff of the API Standards Dept. Copyright API. All rights reserved.

4.2.1 Materials

The work group decided to test one grade of high strength low alloy steel and one grade of precipitation hardenable Nickel based alloy to study the effect of high-pressure hydrogen gas on two distinct material systems. Towards this low alloy steel grade AISI 4140 heat treated via quench and temper treatment to 110 ksi minimum yield was selected and one heat of Alloy 718 solution annealed and aged per API 6ACRA UNS N07718-120K was selected [6]. The details of material selected are given in Table 1 along with chemical composition in Table 2 and Mechanical properties in Table 3. Both the selected heats while very different material grades were of similar size, product form and actual yield strengths. The 4140-110 heat had actual yield strength close to 140 ksi which is typically the max yield strength associated with similar grades such as API 5CT P110 [7].

**Table 1
Description of materials used for testing**

Grade	Product & Size	Condition
4140-110	5" OD bar	Q&T to 110 ksi MY
Alloy 718-120	5" OD bar	Solution annealed and aged per API 6ACRA UNS N07718-120K

**Table 2
Chemical composition (wt%)**

Grade	C	Mn	Si	Cr	Mo	Ni	P	S
4140-110	0.42	0.95	0.26	1.06	0.23	0.18	0.011	0.004
Alloy 718-120	0.013	0.06	0.05	18.2	2.90	53.5	0.008	0.000001

**Table 3
Mechanical Properties of the Material Grades**

Grade	YS, 0.2% offset (ksi)	UTS, (ksi)	% EI	% ROA	Hardness, HRC
4140-110	137.0	154.4	18.0	57.0	35
Alloy 718-120	135.2	181.8	27.6	40.2	38

This document is not an API Standard; it is under consideration within an API technical committee but has not received all approvals required to become an API Standard. It shall not be reproduced or circulated or quoted, in whole or in part, outside of API committee activities except with the approval of the Chairman of the committee having jurisdiction and staff of the API Standards Dept. Copyright API. All rights reserved.

4.2.2 Test Environment

Testing was decided to be done at 100 bar (1450 psi) hydrogen gas pressure at room temperature. The pressure was based on somewhat typical underground hydrogen storage wells pressure especially in salt cavern storage and readily available multiple lab facilities for the anticipated test program duration. Testing at room temperature was done mainly with the reasoning that HE phenomena tends to be more active closer to room temperature for many metallic material grades and room temperature was a good reference to compare different material systems. Testing was done with 99.999% pure dry hydrogen gas with oxygen < 1 ppm and water vapor < 10 ppm and no other intentional impurities. This was selected to baseline a test environment gas for comparison testing. While the effect of impurities is a relevant topic the consensus was to first develop confidence in test methods with more standard test environments and this could be a future consideration.

4.2.3 Test Methods

Below sections provide summary of the test methods; more details are available in Appendix A, B.

4.2.3.1 Slow Strain Rate (SSR)

Testing for Slow Strain Rate via ASTM G142 at target strain rate of 10^{-5} s⁻¹. Based on the scope of testing program; testing for 4140-110 grade was done at Lab A while testing of Alloy 718-120 was done at Lab B^[8]. Testing was to be done with at least three inert specimen and two environmental specimens for each material grade selected.

4.2.3.2 Fracture Toughness

Testing for Fracture Toughness was done via ASTM E1820 via slow rising displacement method using C(T) specimens^[9]. Testing was also to be done at two different labs (A, B) to provide understanding into variation with the test method.

The specimens were extracted at mid-radius location for both grades in the transverse direction and the notch direction was C-L per ASTM E1823^[10]. Testing was to be done with at least one inert specimen and two environmental specimens for each material grade selected. The initial target K-rate of 1 MPa.m^{1/2}.hr⁻¹ (0.01 N.mm^{-3/2}.s⁻¹) for selected for environmental testing while the inert testing K-rate value could be higher.

Lab A used C(T) specimens for both inert and environmental tests with W = 1 inch, B = 0.5 inch. Initial a/W = 0.5 inch (where a is the total crack length including the pre-crack. Nominal notch depth 0.45 inch with 0.05 inch pre-cracking in air) and specimens were side grooved by 5% of the thickness on each side and the samples were side grooved prior to pre-cracking.

Lab B used C(T) specimens for inert tests with W = 2 inch, B = 1 inch while for environmental tests with W = 1.25 inch, B = 0.3 inch. For both cases Initial a/W = 0.5 inch (where a is the total crack length including the pre-crack. Nominal notch depth 0.45 inch with 0.05 inch pre-cracking in air) and specimens were side grooved by 10% of the thickness on each side and the samples were side grooved prior to pre-cracking.

4.2.3.3 Hydrogen Permeation

Hydrogen permeation testing was performed in a specialized stainless-steel high-pressure autoclave test apparatus. Testing was performed using an electrochemical technique per ASTM G148 - Standard Practice for Evaluation of Hydrogen Uptake,

This document is not an API Standard; it is under consideration within an API technical committee but has not received all approvals required to become an API Standard. It shall not be reproduced or circulated or quoted, in whole or in part, outside of API committee activities except with the approval of the Chairman of the committee having jurisdiction and staff of the API Standards Dept. Copyright API. All rights reserved.

Permeation, and Transport in Metals by an Electrochemical Technique [11]. Like SSR testing, permeation testing of 4140-110 grade was done at Lab A while testing of Alloy 718-120 was done at Lab B.

5 Summary of Testing Program Results

5.1 General

The testing scope consisted of performing slow strain rate (SSR) tests, hydrogen permeation tests and rising displacement fracture toughness tests. All environmental tests were performed at room temperature in 100 bar H₂.

5.2 SSR Results

The SSR results for 4140-110 grade performed at strain rate of $1.25 \times 10^{-5} \text{ s}^{-1}$ are shown in Figure 1 (a) summarized in Table 4 (a), (b). While the initial target strain rate was 10^{-5} s^{-1} but the actual testing strain rate ended up being bit higher. Several variables such as ultimate tensile strength (UTS), time to failure (TTF), Total % Elongation, % Plastic Elongation, % reduction in area (RA) as well as the ratio of these variables in hydrogen to in nitrogen (inert) were measured from the test. As shown, except for the UTS, all other variables showed reduction of values for the samples tested in hydrogen with % RA showing the highest drop when compared to inert test results, indicating there is an effect from the high-pressure hydrogen. The specimens tested in H₂ exhibited secondary cracking on the gage length of the specimen as shown in Figure 1 (b).

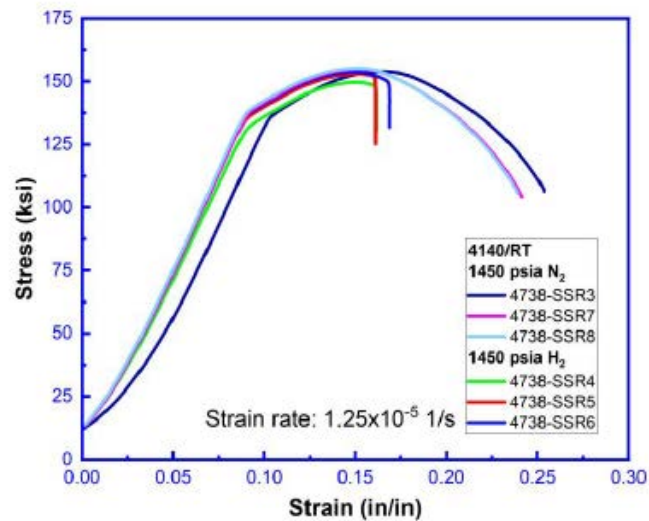


Figure 1 (a) Stress-Strain curves for 4140-110 SSR

This document is not an API Standard; it is under consideration within an API technical committee but has not received all approvals required to become an API Standard. It shall not be reproduced or circulated or quoted, in whole or in part, outside of API committee activities except with the approval of the Chairman of the committee having jurisdiction and staff of the API Standards Dept. Copyright API. All rights reserved.

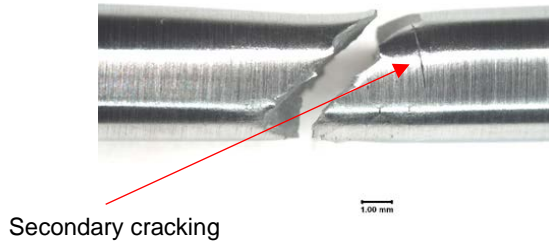


Figure 1 (b) Secondary cracking seen in gage section of 4140-110 H₂ SSR specimen

Table 4 (a) SSR testing results for 4140-110

Env.	UTS (ksi)	TTF (hrs)	Total Elong. (%)	Plastic Elong. (%)	Red. of Area (RA) (%)	Avg. UTS (ksi)	Avg. TTF (hrs)	Avg. Total Elong. (%)	Avg. Plastic Elong. (%)	Avg. RA (%)
N ₂	154.0	5.6	25.0	18.4	55.0	154.7	5.4	24.3	17.7	56.2
N ₂	154.9	5.4	24.1	17.4	56.1					
N ₂	155.2	5.3	23.9	17.2	57.6					
H ₂	149.7	3.6	16.2	7.5	14.0	152.2	3.7	16.4	7.9	12.0
H ₂	153.0	3.6	16.1	7.8	8.2					
H ₂	153.8	3.8	16.8	8.4	13.9					

Table 4 (b) SSR testing results for 4140-110

Env.	UTS ratio	TTF ratio	Total Elong. ratio	Plastic Elong. ratio	RA ratio	Avg. UTS ratio	Avg. TTF ratio	Avg. Total Elong. ratio	Avg. Plastic Elong. ratio	Avg. RA ratio
H ₂	0.97	0.67	0.67	0.42	0.25	0.98	0.69	0.67	0.45	0.21
H ₂	0.99	0.67	0.66	0.44	0.15					
H ₂	0.99	0.70	0.69	0.47	0.25					

The SEM photomicrographs of the 4140-110 steel tested in inert (nitrogen) and hydrogen are shown in Figure 2 and 3 respectively. The SSR specimen fracture surface in inert medium showed ductile behavior with presence of microvoid

This document is not an API Standard; it is under consideration within an API technical committee but has not received all approvals required to become an API Standard. It shall not be reproduced or circulated or quoted, in whole or in part, outside of API committee activities except with the approval of the Chairman of the committee having jurisdiction and staff of the API Standards Dept. Copyright API. All rights reserved.

coalescence showing the material has good ductility in inert environment. The SSR specimen fracture surface in hydrogen test showed a brittle transgranular fracture morphology with secondary cracking. This shows that testing via SSR in presence of H₂ the fracture morphology of 4140-110 changes from ductile to brittle behavior.

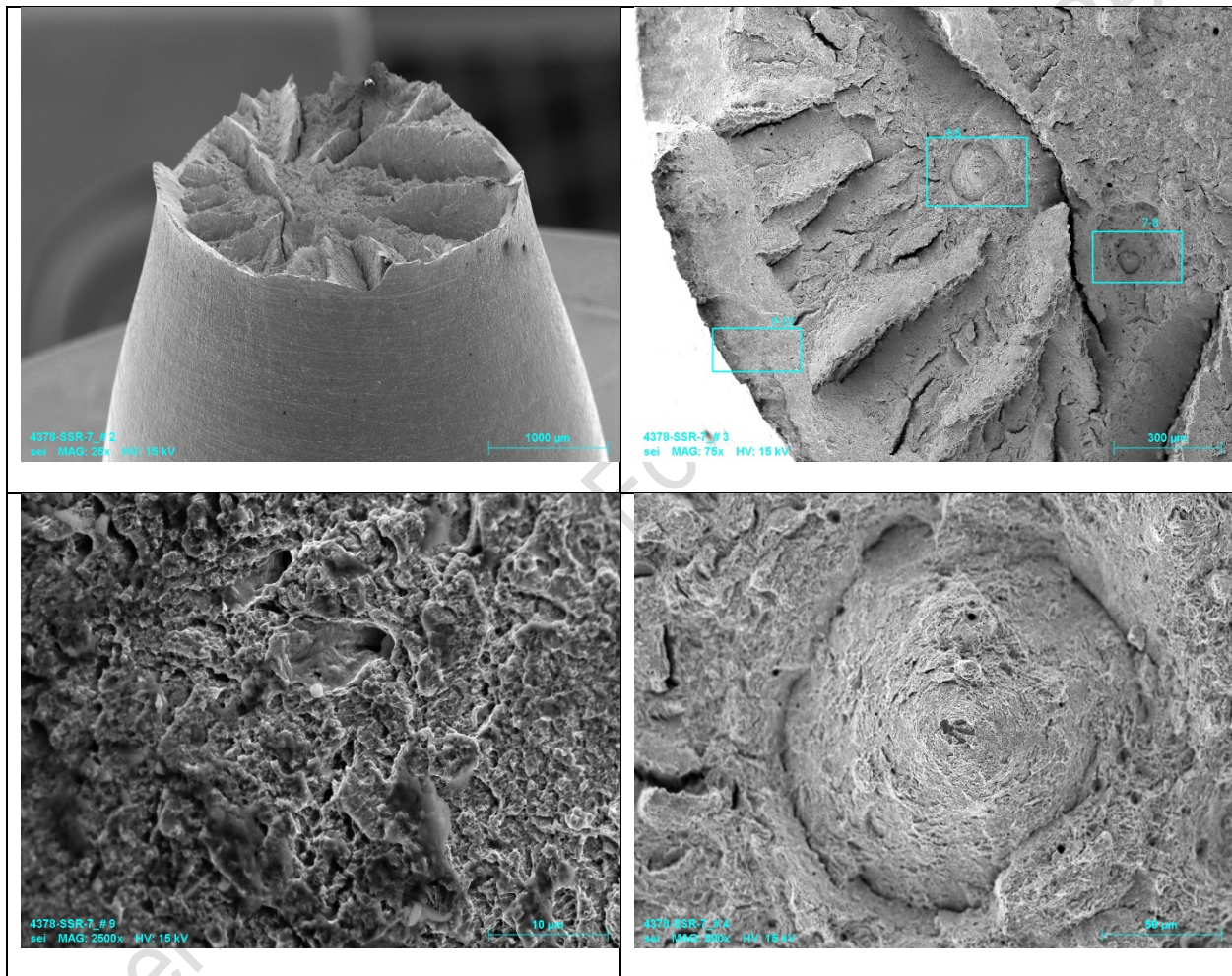


Figure 2 SEM photomicrographs of the SSR sample for 4140-110 steel tested in inert

This document is not an API Standard; it is under consideration within an API technical committee but has not received all approvals required to become an API Standard. It shall not be reproduced or circulated or quoted, in whole or in part, outside of API committee activities except with the approval of the Chairman of the committee having jurisdiction and staff of the API Standards Dept. Copyright API. All rights reserved.

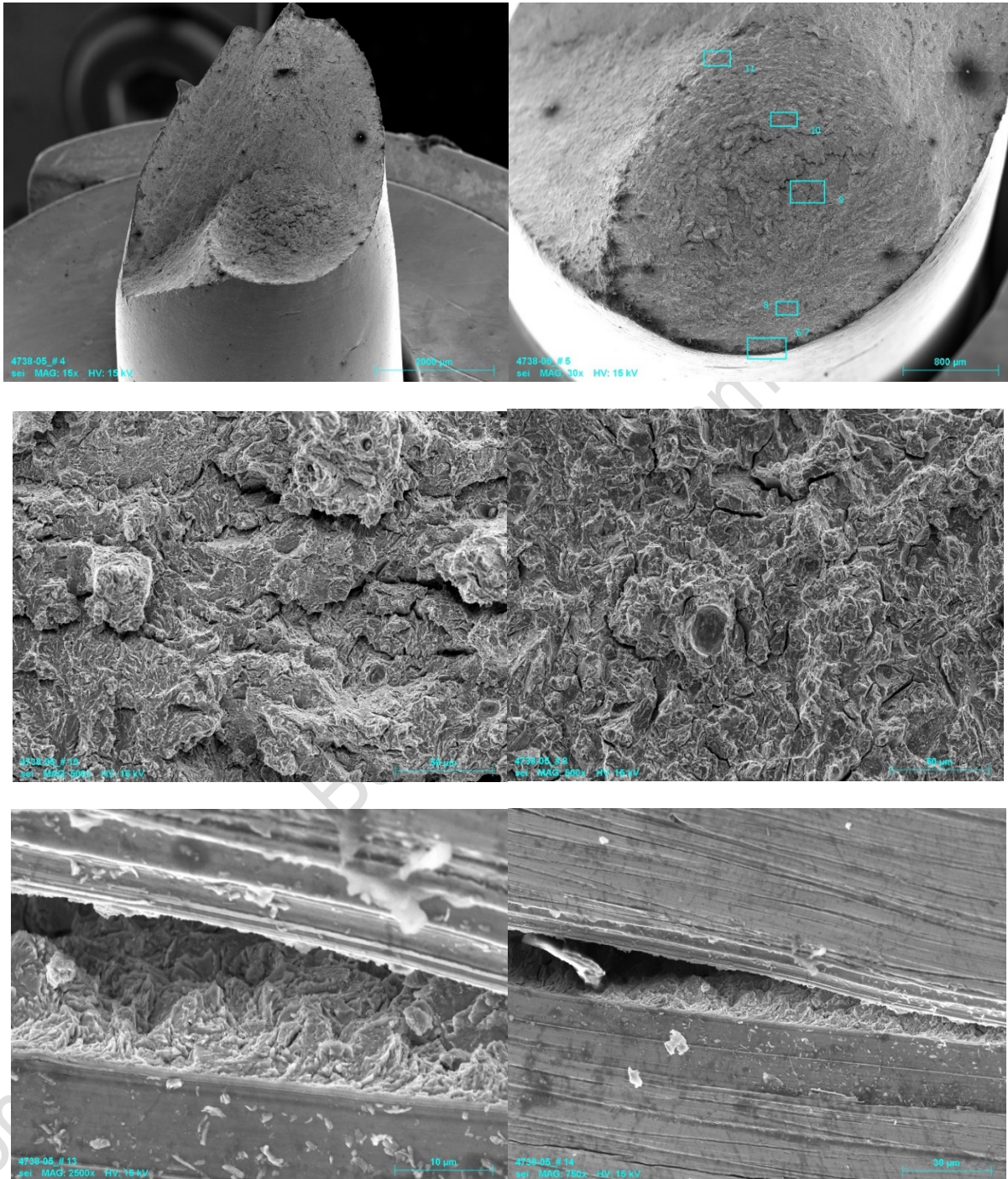


Figure 3 SEM photomicrographs of the SSR sample for 4140-110 steel tested in 100 bar H₂

This document is not an API Standard; it is under consideration within an API technical committee but has not received all approvals required to become an API Standard. It shall not be reproduced or circulated or quoted, in whole or in part, outside of API committee activities except with the approval of the Chairman of the committee having jurisdiction and staff of the API Standards Dept. Copyright API. All rights reserved.

The SSR results for Alloy 718-120 performed at strain rate of $2 \times 10^{-5} \text{ s}^{-1}$. are shown in Figure 4 and summarized in Tables 5(a), (b). While the initial target strain rate was $1 \times 10^{-5} \text{ s}^{-1}$ but the actual testing strain rate ended up being bit higher. Several variables such as ultimate tensile strength (UTS), time to failure (TTF), Total % Elongation, % Plastic Elongation, % reduction in area (RA) as well as the ratio of these variables in hydrogen to in helium (inert) were measured from the test. The hydrogen gas had limited effect on the ultimate tensile stress for the hydrogen tests relative to the helium (inert) tests. The material ductility in terms of elongation, reduction of area was lower in high pressure H_2 compared to inert with the decrease in elongation more than in RA.

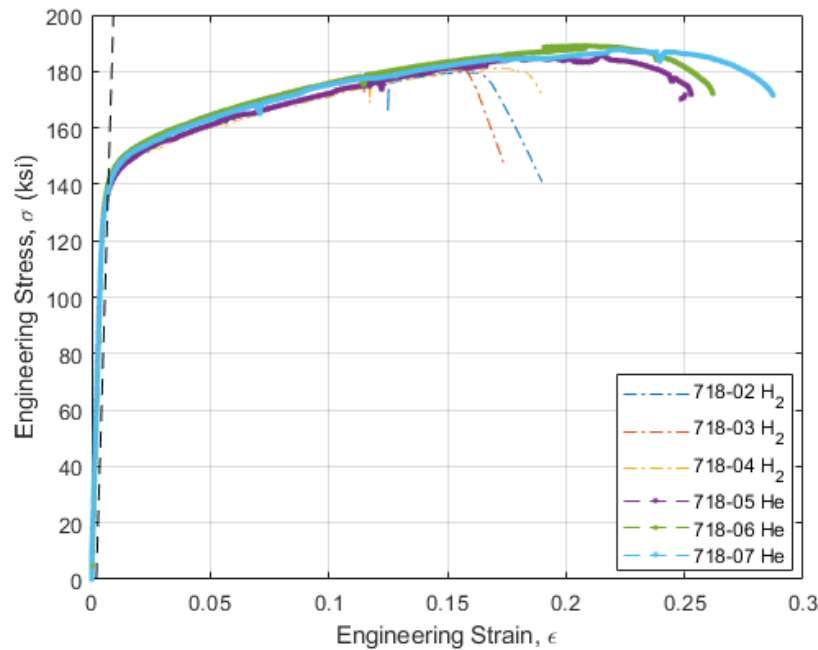


Figure 4 Stress-Strain curves of Alloy 718-120 SSR

Table 5(a) SSR testing results for Alloy 718-120

Env.	UTS (ksi)	TTF (hrs)	Total Elong. (%)	Plastic Elong. (%)	Red. of Area (RA) (%)	Avg. UTS (ksi)	Avg. TTF (hrs)	Avg. Total Elong. (%)	Avg. Plastic Elong. (%)	Avg. RA (%)
He	188.0	3.6	39.0	24.9	26.9	189.0	3.9	38.7	26.3	26.2
He	190.0	3.9	38.3	25.7	27.2					
He	189.0	4.2	38.7	28.3	24.6					
H ₂	180.0	2.3	21.8	15.4	17.4	181.7	2.3	5.5	15.6	20.2
H ₂	183.0	2.2	21.8	15.3	21.1					
H ₂	182.0	2.4	23.5	16.2	22.0					

This document is not an API Standard; it is under consideration within an API technical committee but has not received all approvals required to become an API Standard. It shall not be reproduced or circulated or quoted, in whole or in part, outside of API committee activities except with the approval of the Chairman of the committee having jurisdiction and staff of the API Standards Dept. Copyright API. All rights reserved.

Table 5(b) SSR testing results for Alloy 718-120

Env.	UTS ratio	TTF ratio	Total Elong. ratio	Plastic Elong. ratio	RA ratio	Avg. UTS ratio	Avg. TTF ratio	Avg. Total Elong. ratio	Avg. Plastic Elong. ratio	Avg. RA ratio
H ₂	0.95	0.58	0.56	0.58	0.66	0.96	0.59	0.58	0.59	0.77
H ₂	0.97	0.56	0.56	0.58	0.81					
H ₂	0.96	0.62	0.61	0.62	0.84					

The SEM photomicrographs of Alloy 718-120 tested in inert (helium) and in hydrogen are shown in Figures 5 and 6, respectively. The SSR specimen fracture surface in inert medium showed presence of microvoid coalescence throughout the entire cross section of the fracture surface thus exhibiting a ductile behavior. In case of SSR specimen fracture surface in hydrogen test; the outer circumferential regions showed presence of intergranular fracture morphology with secondary cracking indicating more brittle behavior while the central portion of the specimen showed more ductile behavior with presence of microvoid coalescence. This difference at the two sections may be due to the slower diffusion rate of hydrogen in austenitic microstructure such as Alloy 718-120 [12].

This document is not an API Standard; it is under consideration within an API technical committee but has not received all approvals required to become an API Standard. It shall not be reproduced or circulated or quoted, in whole or in part, outside of API committee activities except with the approval of the Chairman of the committee having jurisdiction and staff of the API Standards Dept. Copyright API. All rights reserved.

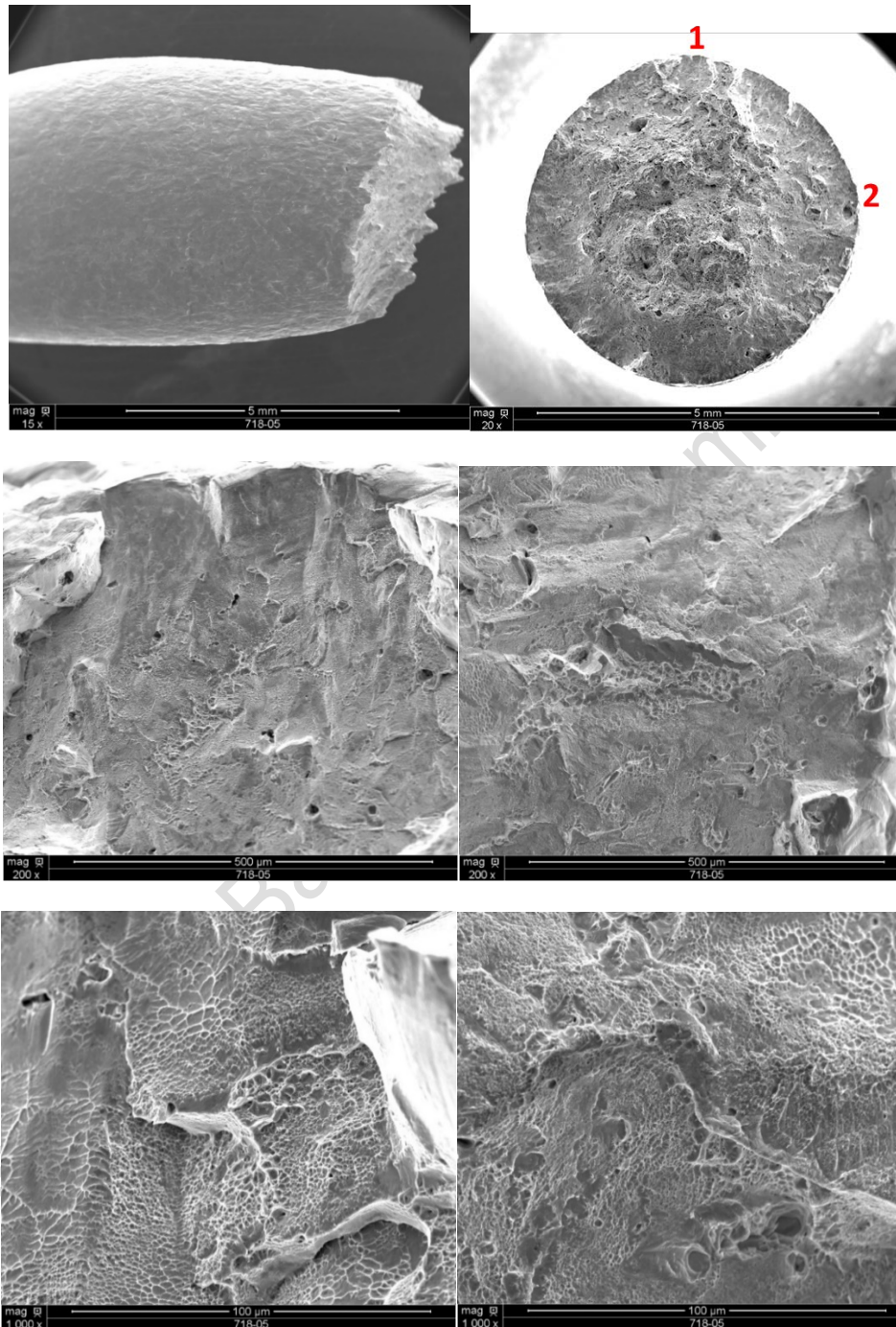


Figure 5 SEM photomicrographs of the SSR sample for Alloy 718-120 tested in inert

This document is not an API Standard; it is under consideration within an API technical committee but has not received all approvals required to become an API Standard. It shall not be reproduced or circulated or quoted, in whole or in part, outside of API committee activities except with the approval of the Chairman of the committee having jurisdiction and staff of the API Standards Dept. Copyright API. All rights reserved.

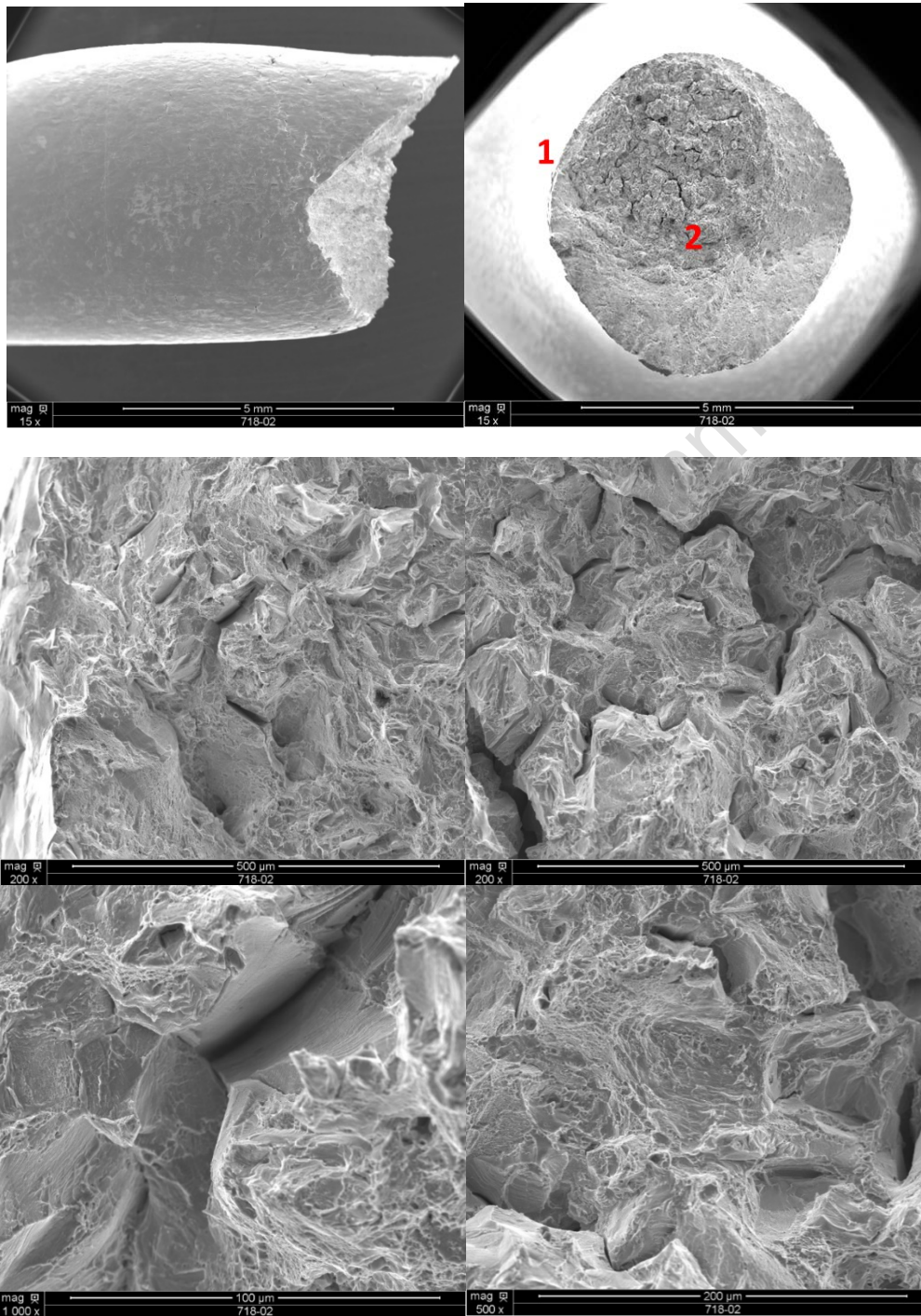


Figure 6 SEM photomicrographs of the SSR sample for Alloy 718-120 tested in 100 bar H₂

This document is not an API Standard; it is under consideration within an API technical committee but has not received all approvals required to become an API Standard. It shall not be reproduced or circulated or quoted, in whole or in part, outside of API committee activities except with the approval of the Chairman of the committee having jurisdiction and staff of the API Standards Dept. Copyright API. All rights reserved.

5.3 FT Results

4140-110 and Alloy 718-120 were tested for fracture toughness evaluation in an inert (nitrogen/air) environment and in 100 bar gaseous hydrogen environment at two different labs (A, B). While the K-rate for H₂ was initially targeted as 0.01 N.mm^{-3/2}.s⁻¹; however, the tested K-rates for the tests in H₂ differed between the two labs. No specific K-rate for inert was specified as the K-values in inert are typically not rate dependent. At Test Lab A, all tests in inert environment (nitrogen) were performed under an initial K rate of approximately 3.8 N.mm^{-3/2}.s⁻¹ whereas the environmental tests were performed at an initial K rate of 0.01 N.mm^{-3/2}.s⁻¹. The inert environmental tests performed at Test Lab B were done under an initial K rate of ~12 N.mm^{-3/2}.s⁻¹. At test lab B the H₂ tests on Alloy 718-120 were performed at an initial K rate of 0.02 N.mm^{-3/2}.s⁻¹ and the tests on 4140-110 steel were done at an initial K rate of 0.003 N.mm^{-3/2}.s⁻¹.

5.3.1 4140-110 results

4140-110 steel was ductile when tested in inert environment but showed a more brittle behavior when tested in hydrogen with the samples breaking in two halves with unstable crack extension at relatively low load values and thus J-R curves were not obtained for 4140-110 steel samples in hydrogen. Rather, elastic K_{IC} values were calculated following the instructions in ASTM E399/ E1820 for the samples tested in hydrogen. Figure 7 shows Load vs CMOD curve of 4140-110 tested in inert and H₂ at Lab A while Figure 8 shows the same when tested in H₂ at Lab B.

The FT results for 4140-110 from two labs are summarized in Table 6 and also compared in Figure 9 as a function of the K rates.. The toughness values in H₂ show clear dependency on the K-rates at which the tests were performed with lower K-rates leading to lower toughness. The data clearly showed the significant reduction of the toughness for the 4140-110 in 100 bar hydrogen compared to the inert environment.

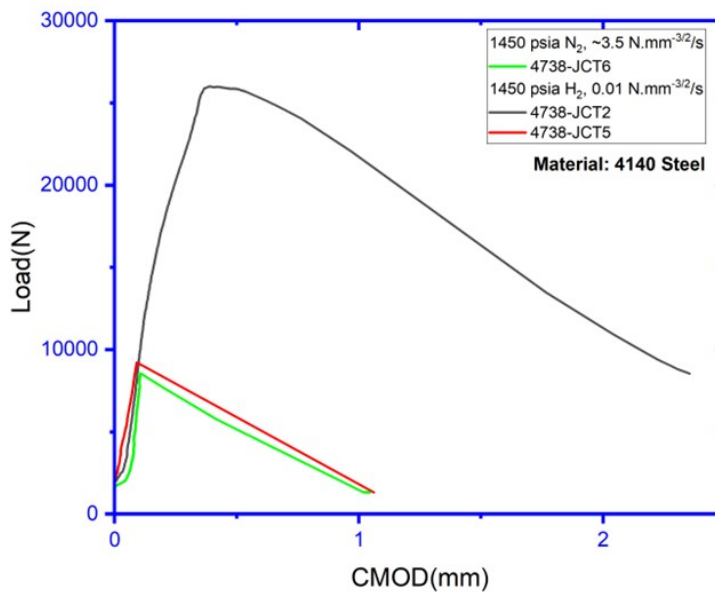


Figure 7 Load vs CMOD for 4140-110 in inert and H₂ from Lab A

This document is not an API Standard; it is under consideration within an API technical committee but has not received all approvals required to become an API Standard. It shall not be reproduced or circulated or quoted, in whole or in part, outside of API committee activities except with the approval of the Chairman of the committee having jurisdiction and staff of the API Standards Dept. Copyright API. All rights reserved.

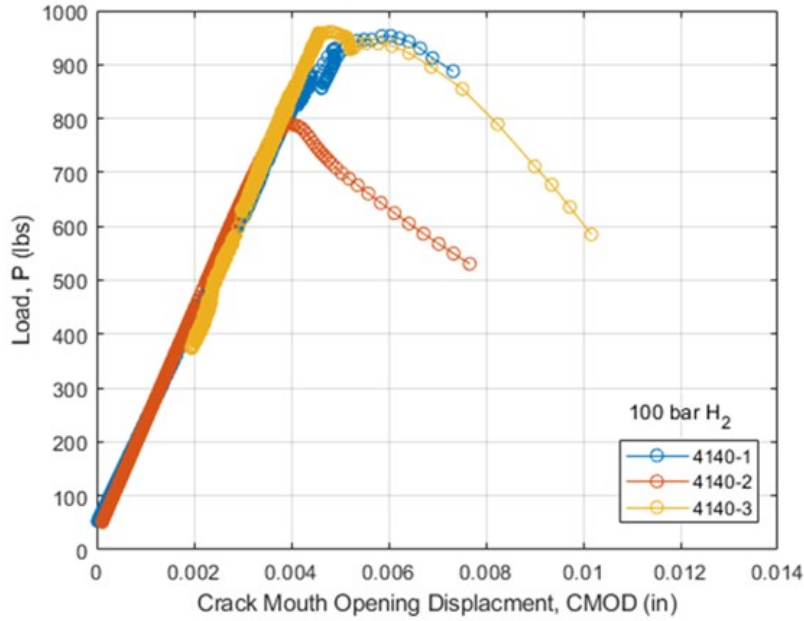


Figure 8 Load vs CMOD for 4140-110 in H₂ from Lab B

Table 6 Summary of FT results for 4140-110

Grade	dk/dt (N.mm ^{-3/2} .s ⁻¹)	K _{IC} (ksi.in ^{1/2})	Test Lab	Env
4140-110	3.8	162.9	A	Inert
	12	149.6	B	Inert
	0.01	42.7	A	H ₂
	0.01	43.0	A	H ₂
	0.003	30.1	B	H ₂
	0.003	26.2	B	H ₂
	0.003	26.2	B	H ₂

This document is not an API Standard; it is under consideration within an API technical committee but has not received all approvals required to become an API Standard. It shall not be reproduced or circulated or quoted, in whole or in part, outside of API committee activities except with the approval of the Chairman of the committee having jurisdiction and staff of the API Standards Dept. Copyright API. All rights reserved.

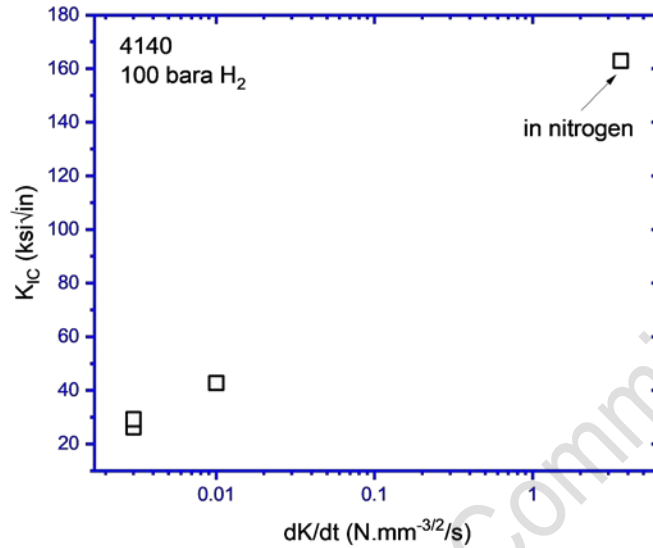


Figure 9 Comparing fracture toughness of 4140-110 in 100 bar H₂ vs K-rate

5.3.2 Alloy 718-120 results

The J-R curves for Alloy 718-120 are shown in Figures 10, 11. The FT results for Alloy 718-120 from two labs are summarized in Table 7. The FT results obtained at the test labs are plotted as a function of the K-rates and compared to the results obtained in the inert environments as well. The comparison is shown in Figure 12 for Alloy 718-120. The comparison clearly showed the significant reduction of the toughness in 100 bar hydrogen compared to the inert environment. The toughness values also showed clear dependency on the K-rates at which the tests were performed. Lower toughness values were observed at lower K-rates, as shown in both Table 7 and Figure 12.

This document is not an API Standard; it is under consideration within an API technical committee but has not received all approvals required to become an API Standard. It shall not be reproduced or circulated or quoted, in whole or in part, outside of API committee activities except with the approval of the Chairman of the committee having jurisdiction and staff of the API Standards Dept. Copyright API. All rights reserved.

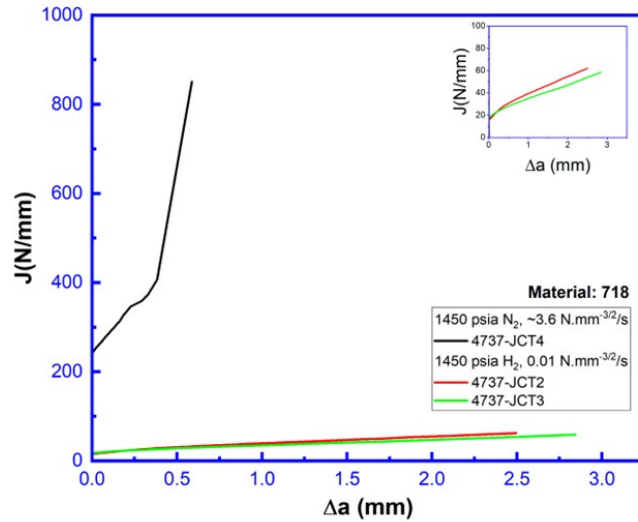


Figure 10 J-R curves for Alloy 718-120 in inert and H₂ from Lab A

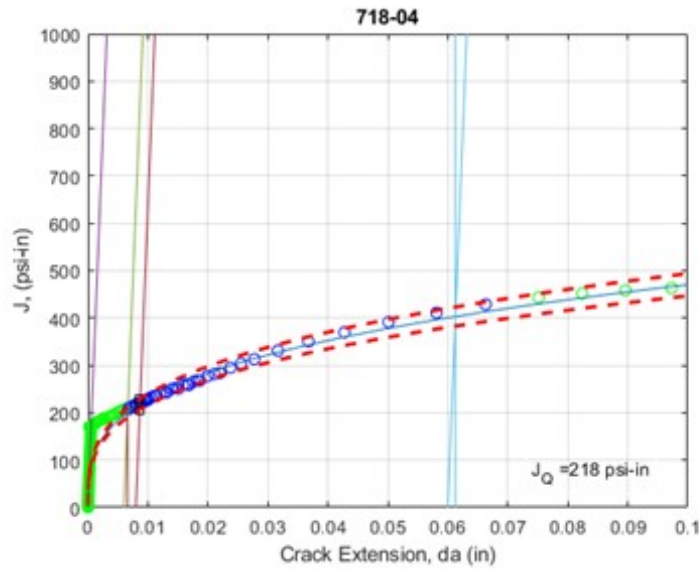


Figure 11 J-R curves for Alloy 718-120 in H₂ from Lab B

This document is not an API Standard; it is under consideration within an API technical committee but has not received all approvals required to become an API Standard. It shall not be reproduced or circulated or quoted, in whole or in part, outside of API committee activities except with the approval of the Chairman of the committee having jurisdiction and staff of the API Standards Dept. Copyright API. All rights reserved.

Table 7 Summary of FT results for Alloy 718-120

Grade	dk/dt ($N.mm^{-3/2}.s^{-1}$)	J_{0mm} ($N.mm^{-1}$)	$J_{0.2mm}$ ($N.mm^{-1}$)	J_{1mm} ($N.mm^{-1}$)	K_{J0mm} ($ksi.in^{1/2}$)	$K_{J0.2mm}$ ($ksi.in^{1/2}$)	K_{J1mm} ($ksi.in^{1/2}$)	Test Lab	Env
Alloy 718-120	3.8	240.4	246.4		210.6	213.2		A	Inert
	0.01	15.8	23.0	39.5	53.9	65.2	85.4	A	H ₂
	0.01	18.1	23.4	35.2	57.8	65.6	85.6	A	H ₂
	0.02	33.8	40.5	70.3	78.9	86.4	113.9	B	H ₂
	0.02	31.3	38.2	61.4	76.0	83.9	106.4	B	H ₂

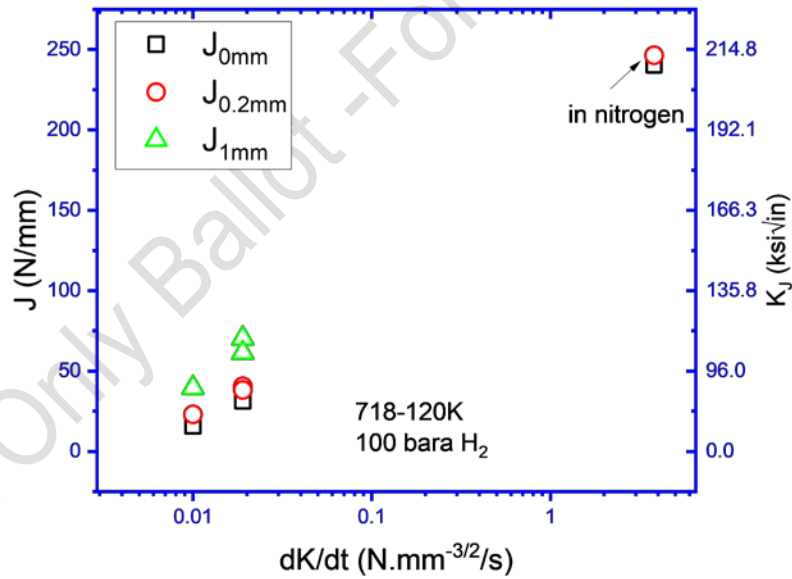


Figure 12 FT results as function of K rates for 718-120 in 100 bar H_2

5.4 Hydrogen Permeation Results

5.4.1 41XX-110

The hydrogen flux experimental setup was validated by performing a hydrogen permeation test using 3.5% NaCl (pH 8.2) on the charging side of the setup. A cathodic potential of -1050 mV vs. SCE was applied to the sample on the charging side which was an X52 line pipe steel. The oxidation side was the typical 0.1 M NaOH solution and was maintained at +300 mV vs. saturated calomel electrode (SCE). The purpose of this test was to make sure the use of a metal autoclave on the charging side, and the use of the fixtures mounting the sample to hold pressure, did not interfere with any hydrogen uptake or the measurements. The flux transient from this validation test is shown in Figure 13. The red line is the numerical fitted line based on the solution to a one-dimensional diffusion and the symbols are the experimental data. As shown, the experimental data and the fitted line agreed very well and the effective diffusion coefficient of hydrogen in the tested material was $9.4 \times 10^{-8} \text{ cm}^2 \cdot \text{s}^{-1}$. The experimental results confirmed that the experimental setup can measure the hydrogen that diffuses through the sample.

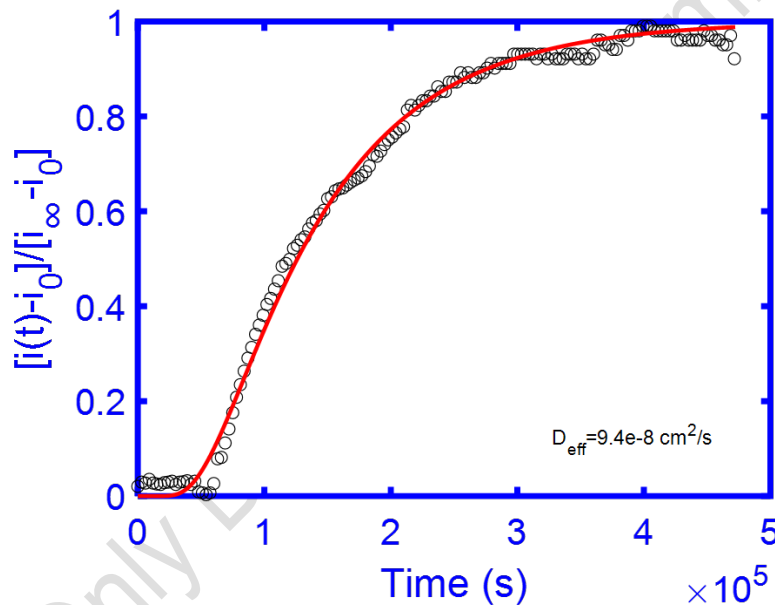


Figure 13 The flux transient as a function of time for the test in 3.5% NaCl solution at pH 8.2

Figure 14 shows the oxidation current as a function of time for the hydrogen flux test that was performed for this project on 4140-110 steel sample. Prior to exposing the sample to hydrogen, a background current density about $12 \text{ nA} \cdot \text{cm}^{-2}$ was established on the oxidation side (exposed to 0.1 M NaOH and polarized to 0.3 V vs. SCE). Hydrogen pressure on the charging side was established. The measured current showed an increase at about 5.2 hours after the sample was exposed to high pressure hydrogen, suggesting hydrogen breaking through the sample and was detected on the oxidation side. The data was analyzed using the same method for the SWCP data based on the solution to a one-dimensional diffusion and compared in Figure 15. As shown, the experimental data agree well with the fitted line and the effective diffusion coefficient in the tested material is $4.63 \times 10^{-7} \text{ cm}^2 \cdot \text{s}^{-1}$.

This document is not an API Standard; it is under consideration within an API technical committee but has not received all approvals required to become an API Standard. It shall not be reproduced or circulated or quoted, in whole or in part, outside of API committee activities except with the approval of the Chairman of the committee having jurisdiction and staff of the API Standards Dept. Copyright API. All rights reserved.

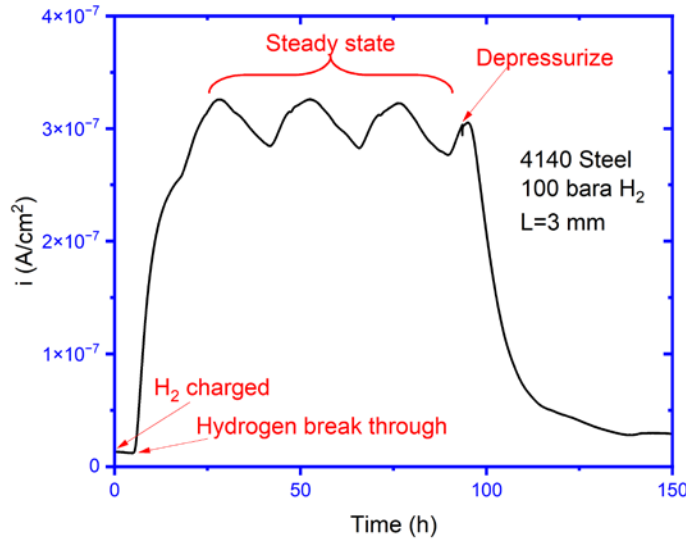


Figure 14 Current vs. time measured in the hydrogen flux test with 4140-110 steel in 100 bar hydrogen

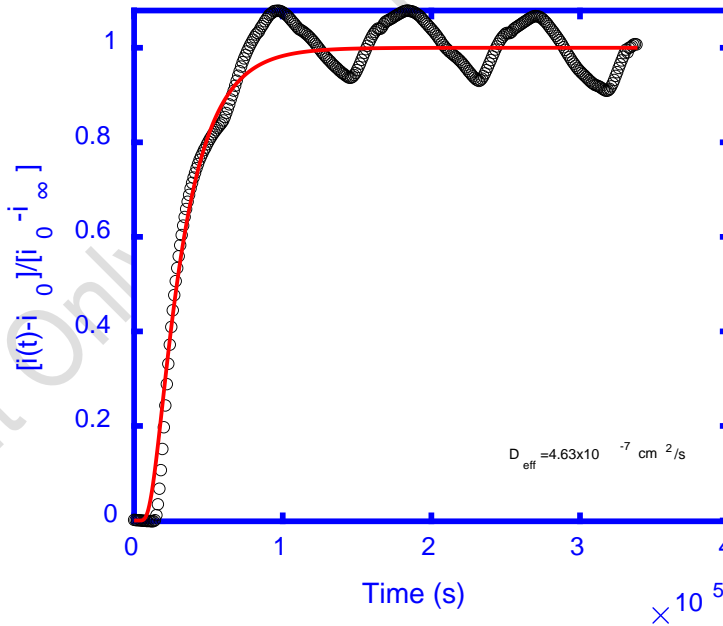


Figure 15 Flux transient measured in the experiment (symbols) and theoretical value (red curve) comparison for the hydrogen flux test with 4140-110 steel in 100 bar hydrogen

This document is not an API Standard; it is under consideration within an API technical committee but has not received all approvals required to become an API Standard. It shall not be reproduced or circulated or quoted, in whole or in part, outside of API committee activities except with the approval of the Chairman of the committee having jurisdiction and staff of the API Standards Dept. Copyright API. All rights reserved.

Figure 16 shows the measured hydrogen flux as a function of time. Using the steady state hydrogen flux and the derived effective hydrogen diffusion coefficient, the subsurface hydrogen concentration was calculated to be about 0.25 ppm.

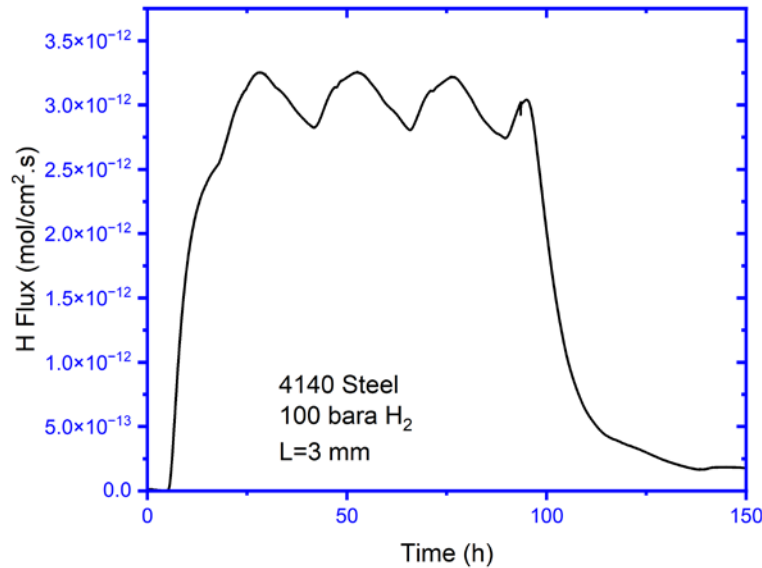


Figure 16 Measured hydrogen flux as a function of time for 4140 steel under 100 bar H₂

5.4.2 Alloy 718-120

The results for the permeation testing for 718-120 grade with 1450 psia hydrogen gas are shown in Figure 17. The figure shows the permeation current density versus time. Low background currents were observed initially (nA range). The hydrogen charging pressure was introduced at 30 hours after the solution in the oxidation cell was transferred. Testing was done for more than three weeks and no increase in the current was observed suggesting the lack of hydrogen breaking through within the duration of testing. It should be noted that the sample thickness for this exposure was 0.118 inches (0.3 cm). Assuming that entry of hydrogen was not a limiting factor and a diffusion coefficient of $2 \times 10^{-11} \text{ cm}^2 \cdot \text{s}^{-1}$ for alloy 718 at RT[23], the breakthrough time for a 0.3 cm thick specimen would be on the order of 35 years. Use of a thinner sample could help in getting hydrogen breakthrough in more reasonable test time but the challenge with a thinner sample (expected to be in micron thickness) would be whether it can be suitable for testing under high pressure hydrogen gas.

This document is not an API Standard; it is under consideration within an API technical committee but has not received all approvals required to become an API Standard. It shall not be reproduced or circulated or quoted, in whole or in part, outside of API committee activities except with the approval of the Chairman of the committee having jurisdiction and staff of the API Standards Dept. Copyright API. All rights reserved.

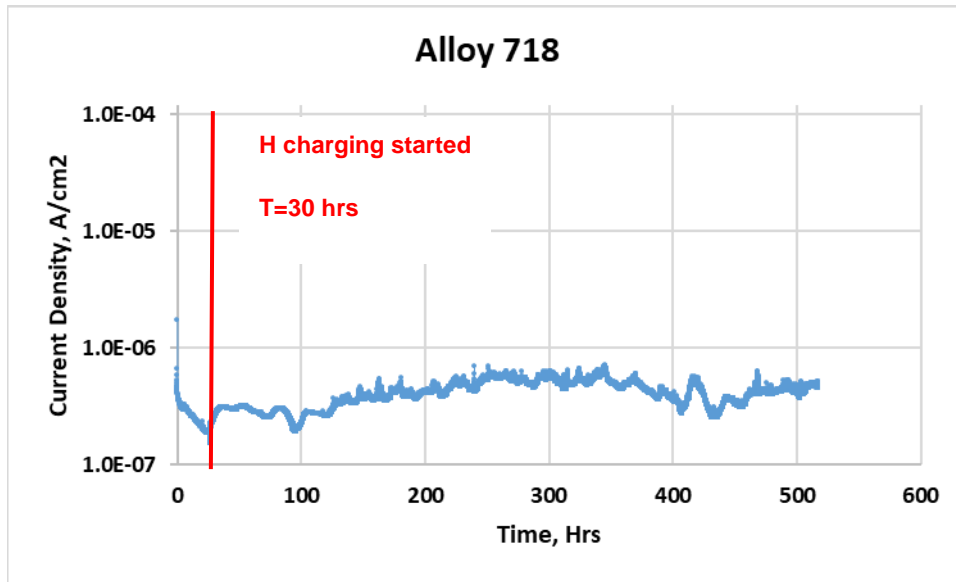


Figure 17 Hydrogen permeation measurements for the Alloy 718-120

6 Discussion

6.1 General

The results of the test program provide measures of susceptibility to hydrogen embrittlement for the materials tested. The results in hydrogen for the two materials from the different test methods are used to understand the role of test method and material type on the susceptibility to hydrogen embrittlement in high pressure H₂.

6.2 Comparison of Materials

The SSR results for both materials showed a decrease in the strain failure and reduction in area in high pressure H₂ compared to inert environments. A comparison of the parameters from the SSR tests for both materials is shown in Figure 18.

This document is not an API Standard; it is under consideration within an API technical committee but has not received all approvals required to become an API Standard. It shall not be reproduced or circulated or quoted, in whole or in part, outside of API committee activities except with the approval of the Chairman of the committee having jurisdiction and staff of the API Standards Dept. Copyright API. All rights reserved.

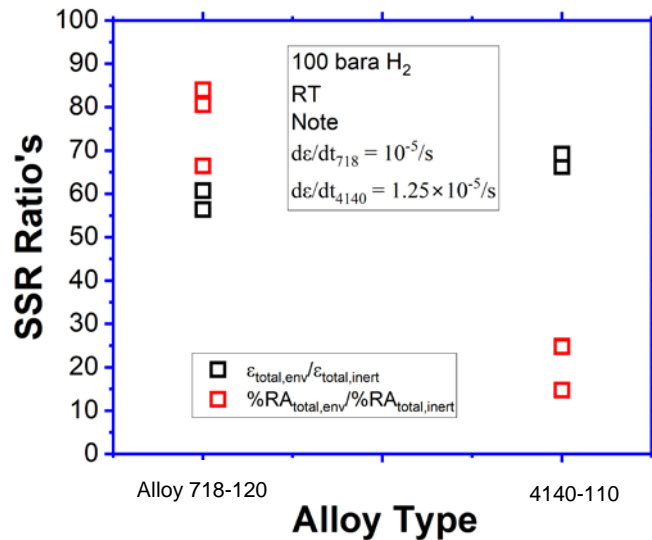


Figure 18 Comparison of the SSR performances in 100 bar H₂ at RT

The comparison clearly suggests that the decrease in %RA (relative to the inert environment) for 4140-110 is significantly higher than for alloy 718-120, even though the change in %total elongation (relative to the inert environment) is similar for both materials. Further SEM done on the fracture surfaces of the SSR specimens for both grades did show more brittle behavior in H₂ compared to their own performance in inert, but Alloy 718-120 did show some ductile features also present in H₂ SSR specimen while 4140-110 H₂ SSR specimen did not show the same. The results suggest that even though the yield strength of the alloys is similar (~140 ksi) the response in the SSR tests is very different, highlighting the difference between the alloy classes.

A comparison of the K_{th} (as defined by J at the onset of crack extension) for the alloys is shown in Figure 19. The results clearly indicate that the K_{th} of Alloy 718 is significantly higher than that of 4140 across the K-rates tested, though it is possible that at very low K-rates the K_{th} of alloy 718 may be lower than the values measured at 0.01 Nmm^{-3/2}.s⁻¹ (the lowest K-rate tested). In addition, to the higher values of K_{th}, alloy 718 exhibited stable crack propagation, while 4140 exhibited unstable crack propagation. This indicates that not only was the K_{th} of 718 higher but the crack growth rate was lower.

Hydrogen permeation studies at 100 bar H₂ showed that for 4140-110 steel the effective diffusion coefficient was measured at 4.63 × 10⁻⁷ cm².s⁻¹ while for Alloy 718-120 no hydrogen breakthrough was possible even after testing for weeks. 4140-110 which is quenched and tempered low alloy steel has a martensitic microstructure while Alloy 718-120 has austenitic microstructure and diffusion of hydrogen through martensitic microstructure is faster than in austenitic microstructure [12].

This document is not an API Standard; it is under consideration within an API technical committee but has not received all approvals required to become an API Standard. It shall not be reproduced or circulated or quoted, in whole or in part, outside of API committee activities except with the approval of the Chairman of the committee having jurisdiction and staff of the API Standards Dept. Copyright API. All rights reserved.

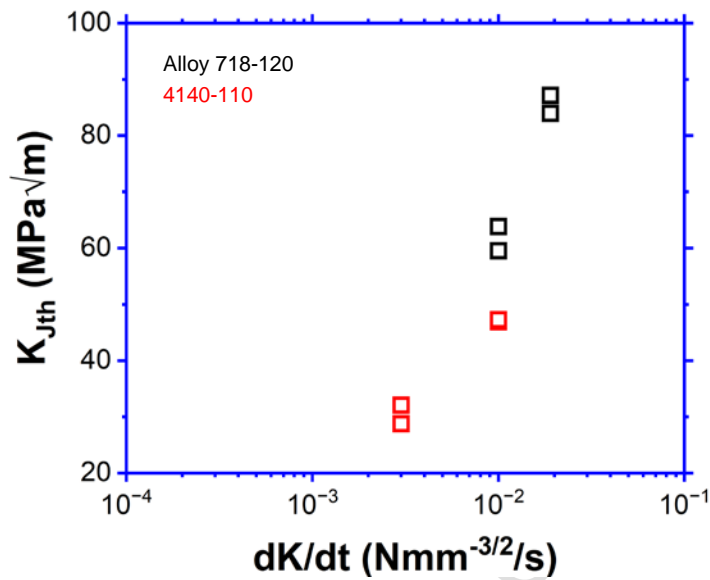


Figure 19 Comparison of the K_{th} values of the two alloys tested in 100 bar H_2 at RT

6.3 Influence of Loading Parameters

The FT results showed that the fracture toughness values of the materials are sensitive to the tested K-rate. In the current work among the K-rates tested for both materials, no plateau in K_{th} was observed. It should be noted some of the differences in K_{th} at different K-rates, may be attributed to the tests at different K-rates being performed at different laboratories.

In order to better understand the effect of K-rate, one of the labs performed an additional test at constant K conditions. The procedure to establish constant K conditions was based on work performed by the lab internally for other projects. The results of the constant K tests at $49.5 \text{ MPa}\cdot\text{m}^{1/2}$ is shown in Figure 20. A very slow SCGR of $2 \times 10^{-9} \text{ mm}\cdot\text{s}^{-1}$ appears to be evident under constant K conditions.

This document is not an API Standard; it is under consideration within an API technical committee but has not received all approvals required to become an API Standard. It shall not be reproduced or circulated or quoted, in whole or in part, outside of API committee activities except with the approval of the Chairman of the committee having jurisdiction and staff of the API Standards Dept. Copyright API. All rights reserved.

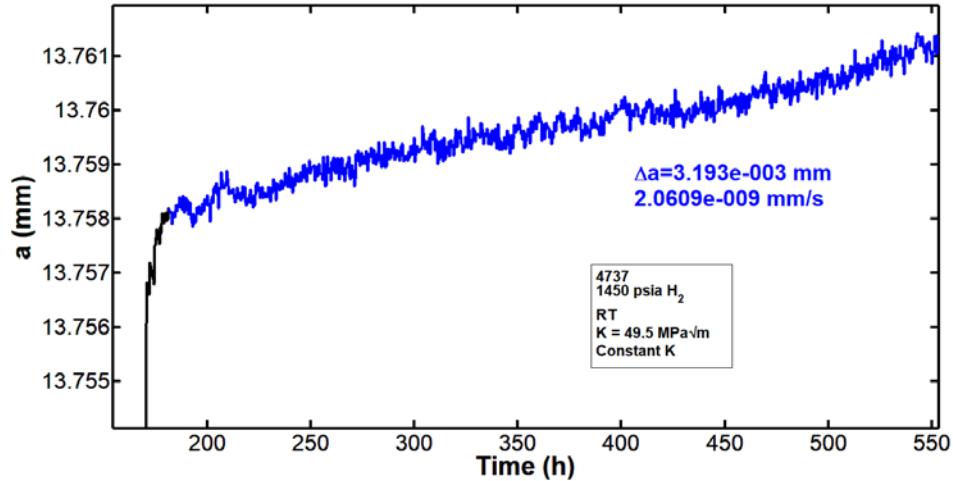


Figure 20 Crack growth rate under constant K conditions ($K = 49.5 \text{ MPa}\cdot\text{m}^{1/2}$) for Alloy 718-120

The SCGR at $60.5 \text{ MPa}\cdot\text{m}^{1/2}$ under constant K conditions is shown in Figure 21. The SCGR is about $2.6 \cdot 10^{-6} \text{ mm}\cdot\text{s}^{-1}$, a 1000-fold increase from the SCGR at $49.5 \text{ MPa}\cdot\text{m}^{1/2}$ suggesting that the K_{th} could be around $49.5 \text{ MPa}\cdot\text{m}^{1/2}$ under constant K or very low K-rate conditions.

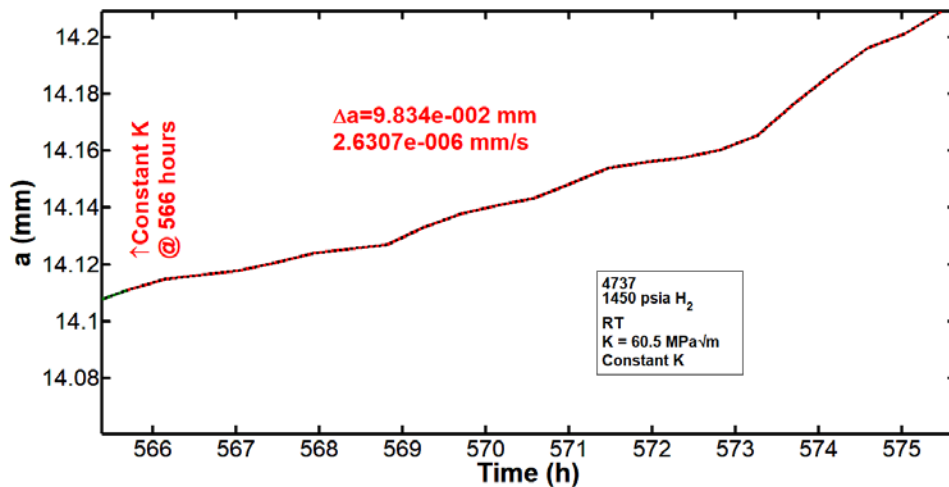


Figure 21 Crack growth rate under constant K conditions ($K = 60.5 \text{ MPa}\cdot\text{m}^{1/2}$) for Alloy 718-120

The results of the constant K tests performed further help understand the role of K-rate on the K_{th} behavior of Alloy 718-120 in high pressure H_2 . A summary of the effect of K-rate on the measured K_{th} for Alloy 718-120 is shown in

This document is not an API Standard; it is under consideration within an API technical committee but has not received all approvals required to become an API Standard. It shall not be reproduced or circulated or quoted, in whole or in part, outside of API committee activities except with the approval of the Chairman of the committee having jurisdiction and staff of the API Standards Dept. Copyright API. All rights reserved.

Figure 22. These results indicate that for Alloy 718-120 under these conditions, the constant K conditions appear to provide lower K_{th} values than the K-rates used for testing in this program. It is possible that slow rising displacement at K-rates of $0.005 \text{ Nmm}^{-3/2} \cdot \text{s}^{-1}$ or less (lower than used in this test program) may provide a sufficiently low K-rate to provide lower bound values of K_{th} and that low K-rates for FT testing in general (while ensuring practicality of the tests) could be used to obtain more conservative fracture toughness values for materials.

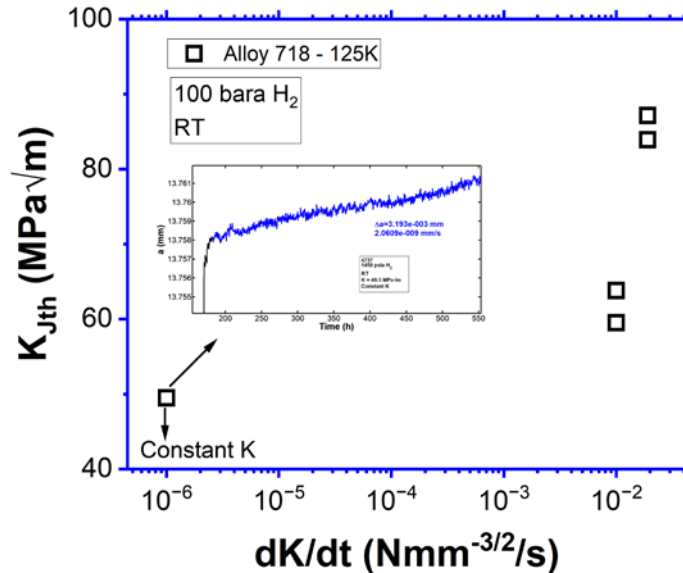


Figure 22 Effect of K-rate on the K_{th} behavior of Alloy718-120 in 100 bar H_2 at RT

6.4 Summary

Overall, the test program showed that metallic materials could see reduction in ductility, toughness under high pressure H_2 that can be relevant to underground storage applications compared to inert behavior of the same material. Additionally, materials with similar yield strength but different microstructure have different retained ductility, fracture toughness. Currently, no specific acceptance criteria or qualification test method exists for choosing materials in these applications. The intent of this test program was to obtain data using relevant test methods while using the learnings of current program as input into future ones. One of the inputs for future test programs that can be relevant is using a lower K-rate for FT testing of metallic materials to further refine fracture toughness values of materials in high pressure H_2 .

Bibliography

1. N. S. Muhammed, B. Haq, D. Al Shehri, A. Al-Ahmed, M. M. Rahman, and E. Zaman, "A review on underground hydrogen storage: Insight into geological sites, influencing factors and future outlook," Energy Reports, vol. 8, pp. 461-499, 2022/11/01/ 2022.

This document is not an API Standard; it is under consideration within an API technical committee but has not received all approvals required to become an API Standard. It shall not be reproduced or circulated or quoted, in whole or in part, outside of API committee activities except with the approval of the Chairman of the committee having jurisdiction and staff of the API Standards Dept. Copyright API. All rights reserved.

2. E. R. Okoroafor, S. D. Saltzer, and A. R. Kavscek, "Toward underground hydrogen storage in porous media: Reservoir engineering insights," *International Journal of Hydrogen Energy*, vol. 47, no. 79, pp. 33781-33802, 2022.
3. B. Pan, X. Yin, Y. Ju, and S. Iglauer, "Underground hydrogen storage: Influencing parameters and future outlook," *Adv Colloid Interface Sci*, vol. 294, p. 102473, Aug 2021.
4. A. Małachowska, N. Lukasik, J. Mioduska and J. Gebicki, "Hydrogen Storage in Geological Formations - The Potential of Salt Caverns," *Energies* 2022, 15(14): 5038.
5. A. Haratian, S.E. Meybodi, M. Dehvedar, "A comprehensive review on the feasibility of largescale underground Hydrogen storage in geological structures with concentration on salt caverns," 6th International Conference on Applied Researches in Science and Engineering, Germany 2022.
6. API 6ACRA "Age-hardened Nickel-based Alloys for Oil and Gas Drilling and Production Equipment"
7. API 5CT "Casing and Tubing"
8. ASTM G142 "Standard Test Method for Determination of Susceptibility of Metals to Embrittlement in Hydrogen Containing Environments at High Pressure, High Temperature, or Both"
9. ASTM E1820 "Standard Test Method for Measurement of Fracture Toughness"
10. ASTM E1823 "Standard Terminology Relating to Fatigue and Fracture Testing"
11. ASTM G148 "Standard Practice for Evaluation of Hydrogen Uptake, Permeation, and Transport in Metals by an Electrochemical Technique"
12. S.D. Pu, A. Turk, S. Lenka, S.W. Ooi "Study of hydrogen release resulting from the transformation of austenite into martensite", *Materials Science and Engineering: A*, vol. 754, pp. 628-635, 2019

This document is not an API Standard; it is under consideration within an API technical committee but has not received all approvals required to become an API Standard. It shall not be reproduced or circulated or quoted, in whole or in part, outside of API committee activities except with the approval of the Chairman of the committee having jurisdiction and staff of the API Standards Dept. Copyright API. All rights reserved.

Appendix A: Experimental Details for API Material Testing in Hydrogen from Test Lab A

A.1 TEST MATERIALS AND SPECIMENS

A.1.1 Materials

The materials tested in the project were provided by API. The provided Alloy 718-120 and 4140-110 grades were assigned Lab A identification number (ID) of 4737 and 4738. Both materials were provided as a bar form with 12 inch in length and 5 inch in outer diameter (OD) for Alloy 718-120 and 17 inch in length and 5 inch in OD for 4140-110 steel. Longer material was provided for 4140-110 steel due to the need of machining SSR samples and flux samples. Table A.1 shows a summary of the material dimensions and the mechanical properties.

Table A.1 Dimensions and mechanical properties of supplied materials

Grade	Lab A ID	Diameter (in)	Length (in)	Yield Strength (ksi)	Tensile Strength (ksi)
Alloy 718-120	4737	5	12	135.2	181.8
4140-110	4738	5	17	137.0	154.4

A.1.2 Specimen Description

A.1.2.1 Slow Strain Rate (SSR) Specimen

SSR tests were performed for 4140-110 grade using the button head SSR samples. An example schematic of the button head SSR sample is shown in Figure A.1. SSR samples were also extracted from the mid-radius location of the bar.

This document is not an API Standard; it is under consideration within an API technical committee but has not received all approvals required to become an API Standard. It shall not be reproduced or circulated or quoted, in whole or in part, outside of API committee activities except with the approval of the Chairman of the committee having jurisdiction and staff of the API Standards Dept. Copyright API. All rights reserved.

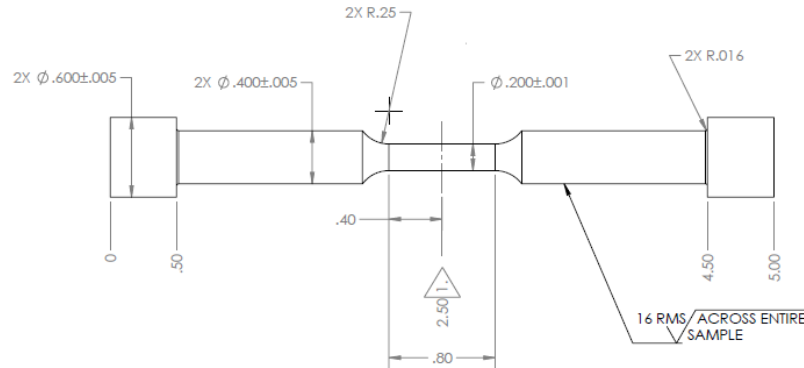


Figure A.1 Schematic of the button head SSR sample

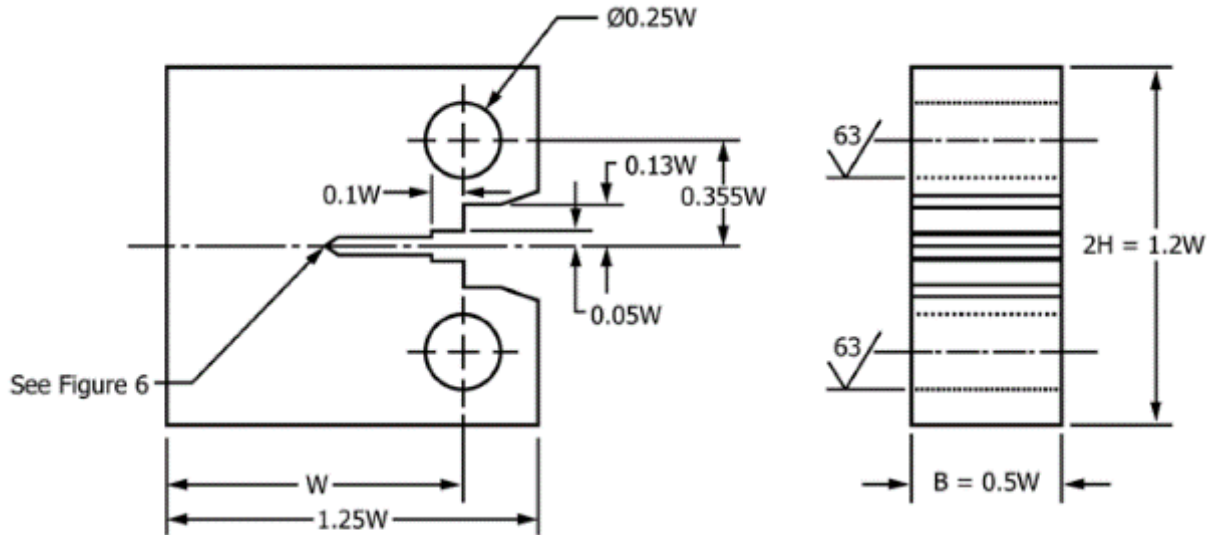
A.1.2.2 Fracture Toughness (FT) Specimen

Compact tension (CT) specimens were used to perform FT testing and were extracted from the provided materials at the mid-radius location (Figure A.2). The samples were notched in the C-L orientation as per ASTM E1823 with the crack growing along the longitudinal direction of the bar

A schematic of the CT fracture toughness specimen (referred as JCT) is shown in Figure A.2. The samples were machined to the following dimensions:

- Specimen width, $W=1$ " (1.25")
- Specimen thickness, $B=0.5$ " (0.3")
- Initial $a/W = 0.5$ (where a is the total crack length including the pre-crack. Nominal notch depth 0.45 inch with 0.05-inch pre-cracking in air) (0.5)
- Specimens were side grooved by 5% of the thickness on each side. The samples were side grooved prior to pre-cracking. (side grooved similarly)

This document is not an API Standard; it is under consideration within an API technical committee but has not received all approvals required to become an API Standard. It shall not be reproduced or circulated or quoted, in whole or in part, outside of API committee activities except with the approval of the Chairman of the committee having jurisdiction and staff of the API Standards Dept. Copyright API. All rights reserved.



Notes:

1. Tolerance on all dimensions $\pm 0.013W$
2. Pin shall be sized so that maximum clearance with hole is $0.02W$

Figure A.2 Schematic of the FT CT specimens (Ref: ASTM E1820)

The samples were pre-cracked in air to an initial a/W of 0.5 under a constant K_{max} of 25 $\text{ksi}\sqrt{\text{in}}$ (27.5 $\text{MPa}\sqrt{\text{m}}$) with R ratios varying from 0.2 to 0.4 and at 2 Hz. The last 15 mils of the pre-cracking were performed under a ΔK of 15 $\text{ksi}\sqrt{\text{in}}$ (16.5 $\text{MPa}\sqrt{\text{m}}$). All pre-cracking was done at Lab A.

A.1.2.3 Hydrogen Permeation Specimen

A disk sample with 3 mm thickness was used in hydrogen flux test, as shown in Figure A.3

This document is not an API Standard; it is under consideration within an API technical committee but has not received all approvals required to become an API Standard. It shall not be reproduced or circulated or quoted, in whole or in part, outside of API committee activities except with the approval of the Chairman of the committee having jurisdiction and staff of the API Standards Dept. Copyright API. All rights reserved.

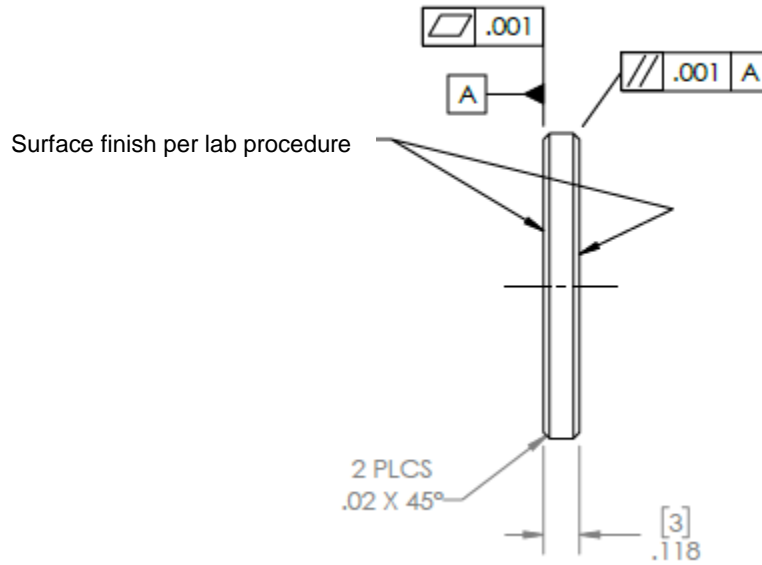


Figure A.3 Dimensions of the hydrogen permeation sample

A.2 Test Matrix

Table A.2 lists the tests that were performed in the project, including the FT tests, SSR tests and the hydrogen flux test.

Table A.2 Test matrix

Material	Type of Testing	Environment	Number of Tests
Lab A ID 4737 (Alloy 718-120)	FT	100 bar nitrogen	1
		100 bar hydrogen, measure oxygen and moisture	2
Lab A ID 4738 (4140-110)	FT	100 bar nitrogen	1
		100 bar hydrogen, measure oxygen and moisture	2
	SSR	100 bar nitrogen	3

This document is not an API Standard; it is under consideration within an API technical committee but has not received all approvals required to become an API Standard. It shall not be reproduced or circulated or quoted, in whole or in part, outside of API committee activities except with the approval of the Chairman of the committee having jurisdiction and staff of the API Standards Dept. Copyright API. All rights reserved.

		100 bar hydrogen, measure oxygen and moisture	3
	H flux	100 bar hydrogen, measure oxygen and moisture	1

A.3 Test Details

The tests in this project were performed using 100% hydrogen to study the environmental effect and in nitrogen to establish the baseline performance in inert environment. All tests were performed at a total pressure of 100 bar and at room temperature.

A.3.1 Environmental Testing procedure

All environmental tests were performed in Alloy C276 (Nickel based alloy) autoclaves. The test specimens were electrically isolated from the autoclave, and the test frame, to prevent ground loops affecting the crack growth measurements. The autoclaves were assembled with the test specimen to be tested, sealed and pressure tested overnight at 2000 psig. After the pressure test, the autoclave/sample was purged with high purity nitrogen overnight to reduce moisture. This was followed by cycles of 150 psig nitrogen and vacuum to remove nitrogen from the previous step. This pressure-release cycle was repeated five more times to minimize oxygen in the system. This was followed by pressurization of the autoclave with test gas - 100% hydrogen to 150 psig and vacuuming out the filled hydrogen. This pressure-release cycle was repeated one more time. This step was followed by flowing the test gas through the autoclave at a pressure of 500 psig at a flow rate of about 0.5 SCFH. The gas outlet from the autoclave was connected to an oxygen analyser. The lines connecting the sensor to the autoclave were also preconditioned using the nitrogen/vacuum and hydrogen/vacuum cycles. Once the oxygen concentration reached below 1 ppm, the autoclave was pressurized to 100 bar and all valves connecting to gas tanks were closed. Along with the oxygen sensor, there was a moisture analyser connected to the autoclave to confirm that the moisture was low enough to validate all results obtained. The system was allowed to stabilize for at least 2 hours before loading the sample at the displacement rate. At the conclusion of the test, the pressure of the autoclave was brought down to ambient by releasing the gas through the oxygen analyser to ensure that the oxygen stayed below 1 ppm during the test.

A.3.2 SSR Testing

SSR tests were performed using servo electric frames which record the load and displacement of the testing samples. All samples were strained until failure. The SSR testing was done at strain rate of $1.25 \times 10^{-5} \text{ s}^{-1}$.

Upon completing the SSR tests, all specimens were removed from the test vessel and the diameter of the sample near the fracture location was measured using a stereomicroscope. This value was used to calculate the reduction in area (RA). The samples were also examined to document any indication of brittle failure or secondary cracking.

A.3.3 FT Testing

The setup is shown in Figure A.4 used for FT using slow rising displacement method. The inert test in nitrogen were performed at a displacement rate of $1 \times 10^{-4} \text{ in.s}^{-1}$ corresponding to a K rate of 3 to 4 $\text{N.mm}^{-3/2}.\text{s}^{-1}$. The tests in nitrogen not only help establish the baseline performance of the materials in an inert environment but also help establish the displacement rate that is required to achieve the K rate for the tests in hydrogen. FT tests in hydrogen performed under

This document is not an API Standard; it is under consideration within an API technical committee but has not received all approvals required to become an API Standard. It shall not be reproduced or circulated or quoted, in whole or in part, outside of API committee activities except with the approval of the Chairman of the committee having jurisdiction and staff of the API Standards Dept. Copyright API. All rights reserved.

displacement control at a low initial K-rate of $0.01 \text{ N}\cdot\text{mm}^{-3/2}\cdot\text{s}^{-1}$ to capture the environmental effect. The crack length in all tests were measured *in-situ* using the Direct Current Potential Drop (DCPD) technique. A constant current of 4 amp was used for DCPD crack length monitoring and the voltage drop across the crack mouth was measured using a high resolution digital multi-meter. The polarity of the current was frequently alternated during each DCPD data point measurement. This was done to eliminate thermal junction potentials in the system and improve the accuracy of DCPD. Ni wires encased in PTFE heat shrink sleeves were used for the current and voltage signals. The spot weld locations of the probes on the samples were coated (using 3M Scotchkote™ 323 liquid epoxy) as a strain relief. The measured voltage drop was converted into crack length using the Johnson equation (equation A1.2 in ASTM E1457). The voltage drops, as well as the converted crack length, were recorded using a Labview® program. Upon completing the FT tests, all specimens were removed from the autoclaves and broken open to examine the fracture surface using a stereomicroscope for measurement of the actual initial and final crack length.

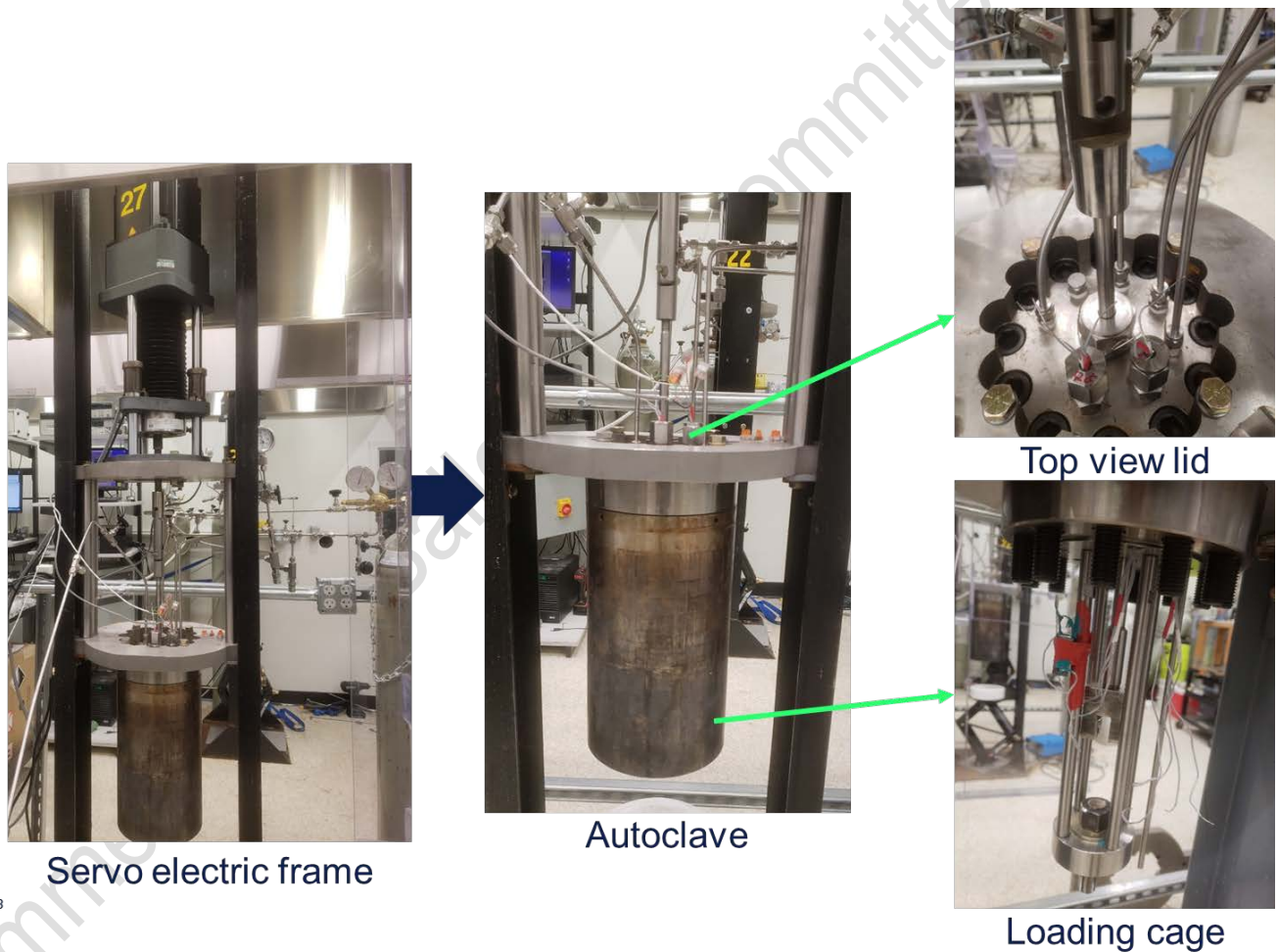


Figure A.4 Test set up showing the test frame, autoclave and the gas cylinders

This document is not an API Standard; it is under consideration within an API technical committee but has not received all approvals required to become an API Standard. It shall not be reproduced or circulated or quoted, in whole or in part, outside of API committee activities except with the approval of the Chairman of the committee having jurisdiction and staff of the API Standards Dept. Copyright API. All rights reserved.

A.3.4 Hydrogen Flux Measurement

Hydrogen flux measurement for permeation was performed using the Devanathan-Stachurski cell technique and the instructions described in ASTM G148. The experimental setup is shown in Figure A.5. The experimental setup consists of a C276 autoclave on the hydrogen charging side and an acrylic cell on the oxidation side.

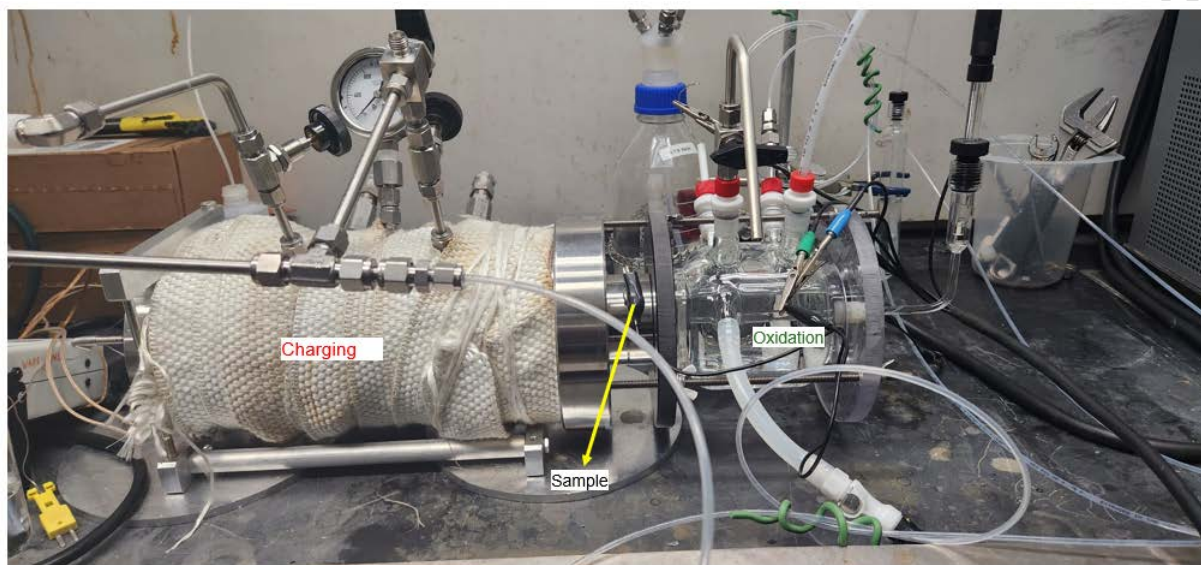


Figure A.5 Hydrogen flux experimental setup

The oxidation cell contains 0.1 M NaOH solution that is constantly purged using high purity nitrogen. A Pt/Nb wire loop and a saturated calomel electrode (SCE), were used as counter and SCE reference electrodes, respectively.

Prior to starting test, the NaOH solution and the oxidation cell were both deaerated with high purity nitrogen overnight. Once the solution and the cell were fully deaerated, the solution was transferred to the oxidation cell under nitrogen pressure to avoid any oxygen ingress into the oxidation cell. The sample then was polarized to 0.3 V vs. SCE while the current was measured to establish a steady background. Typically, a background current density lower than 100 nA/cm² is expected. After the background current density fell below 100 nA/cm², the autoclave was subjected to the same charging procedure as that used in the FT testing and SSR testing. This provided low oxygen and moisture conditions on the charging side and to establish 100 bar hydrogen pressure to begin hydrogen flux measurement. Constant applied potential on the oxidation side would facilitate oxidation of any hydrogen diffusing through the sample from the charging side. When hydrogen diffuses through the testing sample, this would result in a current transient, i.e., current increasing and then reaching a plateau, that could be used to convert to diffusion flux and calculate the hydrogen diffusion coefficient.

This document is not an API Standard; it is under consideration within an API technical committee but has not received all approvals required to become an API Standard. It shall not be reproduced or circulated or quoted, in whole or in part, outside of API committee activities except with the approval of the Chairman of the committee having jurisdiction and staff of the API Standards Dept. Copyright API. All rights reserved.

A.4 Data Analysis

A.4.1 SSR Data Analysis

SSR data was analysed to determine the various parameters such as Time to Failure, % Plastic Elongation, % Reduction of Area etc. in accordance with the instructions in NACE TM0198, ASTM G142.

A.4.2 FT Data Analysis

The data from the FT tests was analyzed using ASTM E1820. The fracture toughness J was calculated from the sum of the elastic and plastic components according to equations (1) to (3) below:

$$J_{tot} = J_{el} + J_{pl} \quad (1)$$

$$J_{tot} = \frac{K^{(i)2}(1-\nu^2)}{E} + J_{pl(i)} \quad (2)$$

$$J_{pl(i)} = \left[J_{pl(i-1)} + \left(\frac{\eta_{pl(i-1)}}{b_{(i-1)}} \right) \frac{A_{pl(i)} - A_{pl(i-1)}}{BN} \right] \left[1 - \gamma_{(i-1)} \left(\frac{a_{(i)} - a_{(i-1)}}{b_{i-1}} \right) \right] \quad (3)$$

where:

i : step

K : Stress Intensity Factor (N·mm^{-3/2})

$$K = \frac{P}{(BB_N W)^{1/2}} f\left(\frac{a}{W}\right)$$

P : load (N)

ν : Poisson's Ratio, 0.32

E : Young's Modulus (MPa): assumed to be 200138 MPa (29000 ksi)

$$\eta_{pl(i-1)} = 2 + 0.522b_{(i-1)} / W$$

$$\gamma_{pl(i-1)} = 1 + 0.76b_{(i-1)} / W$$

A_{pl} : Plastic component of the area under the Load CMOD curve (based on ASTM E1820 A2.4.2.2, equations A2.9, A2.10 and A2.11)

B : Sample thickness (mm)

This document is not an API Standard; it is under consideration within an API technical committee but has not received all approvals required to become an API Standard. It shall not be reproduced or circulated or quoted, in whole or in part, outside of API committee activities except with the approval of the Chairman of the committee having jurisdiction and staff of the API Standards Dept. Copyright API. All rights reserved.

B_N : Sample thickness at the root of side grooves (mm)

W : Sample width (mm)

a : Crack length (mm)

b : Remaining ligament (mm), $W-a$

The processed J vs. Δa was fitted to equation (4) below:

$$J = A_J \Delta a^\beta \quad (4)$$

The fitting parameters, J at 0 mm (point of first crack extension), 0.2 mm and 1 mm of crack extension and the J value at the maximum load are reported. **The value J_{maxload}** is the derived at the maximum force. These J values were also converted to K_J using equation (5) below:

$$K_J = \sqrt{\frac{JE}{1-\nu^2}} \quad (5)$$

A.4.3 Hydrogen Flux Data Analysis

In the case hydrogen diffusion does occur, and hydrogen oxidation current is measured, the rising transient of the sample can be expressed by the following equation:

$$\frac{i_t - i_0}{i_\infty - i_0} = \frac{2L}{\sqrt{\pi Dt}} \sum_{n=0}^{\infty} \exp\left(-\frac{(2n+1)^2 L^2}{4Dt}\right) \quad (6)$$

Where: i_t – transient current at time t (A/cm^2)

i_0 – initial current at $t=0$ (A/cm^2)

i_∞ – steady state current at $t \rightarrow \infty$

L – sample thickness (cm)

t – time (s)

D – diffusion coefficient (cm^2/s)

A Matlab script was used to do a regression and generate flux data and calculate the diffusion coefficient.

This document is not an API Standard; it is under consideration within an API technical committee but has not received all approvals required to become an API Standard. It shall not be reproduced or circulated or quoted, in whole or in part, outside of API committee activities except with the approval of the Chairman of the committee having jurisdiction and staff of the API Standards Dept. Copyright API. All rights reserved.

Appendix B: Experimental Details for API Material Testing in Hydrogen from Test Lab B

B.1 MATERIALS AND SPECIMEN GEOMETRIES

Two material grades were provided for evaluation in low-alloy steel 4140 quenched and tempered to 110 ksi MY and Alloy 718-120 per API 6ACRA UNS N07718-120K were provided. The materials were nominally 5 inches in diameter and sufficient quantities were provided to fabricate all necessary specimens and spares. The material forms and nominal tensile properties as provided in the material test reports are provided in Table B.1

Table B.1 Material forms and tensile properties from material testing reports provided by API

Grade	Form	0.2% Yield Stress (ksi)	Ultimate Tensile Stress (ksi)	Elongation (%)	Reduction of Area (%)
4140-110	5-inch round	142.1	157.9	18.9	57.9
Alloy 718-120	5-inch round	135.2	181.8	27.6	40.2

All test specimens were excised at the mid-radius. The slow strain rate tensile (SSR) bars were oriented in the longitudinal (axial) direction and fracture toughness specimens were oriented in the transverse direction with C-L notch orientation. Test specimens were fabricated as outlined in ASTM G142 for SSR as shown in Figure B.1.

Two different compact tension (CT) specimen geometries per ASTM E1820 were utilized for the fracture toughness (FT) testing. The air specimens were larger due to a higher anticipated fracture toughness in the absence of hydrogen (width (W) equal to 2 inches and thickness (B) equal to 1 inch) as shown in Figure B.2. This larger specimen ensured valid test results and J-dominance. The hydrogen test specimens were fabricated to be compatible with existing autoclave hardware (W of 1.25 inches and B of 0.30 inches) as shown in Figure B.3. After fatigue pre-cracking, the specimens were side grooved nominally 20% total in the thickness dimension (10% on each side).

A permeation membrane was machined from the Alloy 718-120 for permeation studies. The sample was removed from mid-radius location. The rectangular membrane had dimensions of 1.55 inches width, 1.76 inches length, and was 0.118 inches (3 mm) in thickness as seen in Figure B.4 The one side that would be exposed to the oxidation cell (detection side) was coated with Pd prior to testing.

This document is not an API Standard; it is under consideration within an API technical committee but has not received all approvals required to become an API Standard. It shall not be reproduced or circulated or quoted, in whole or in part, outside of API committee activities except with the approval of the Chairman of the committee having jurisdiction and staff of the API Standards Dept. Copyright API. All rights reserved.

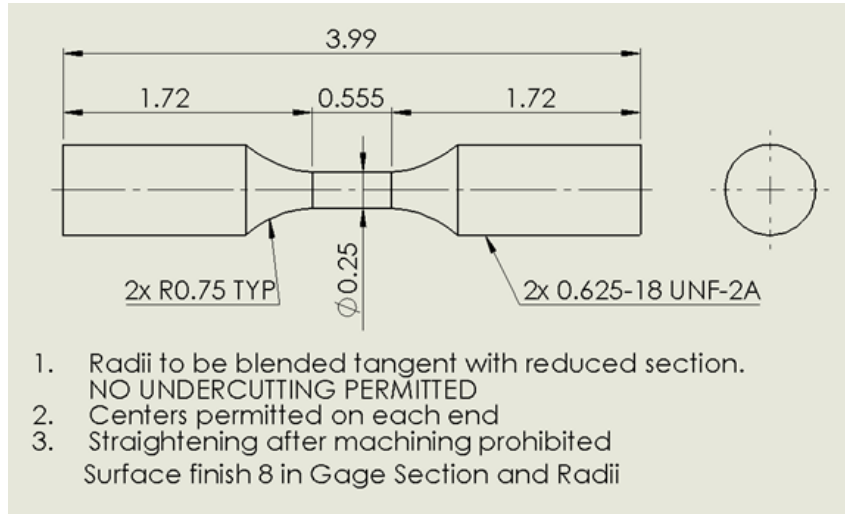


Figure B.1 Slow Strain Rate specimen geometry

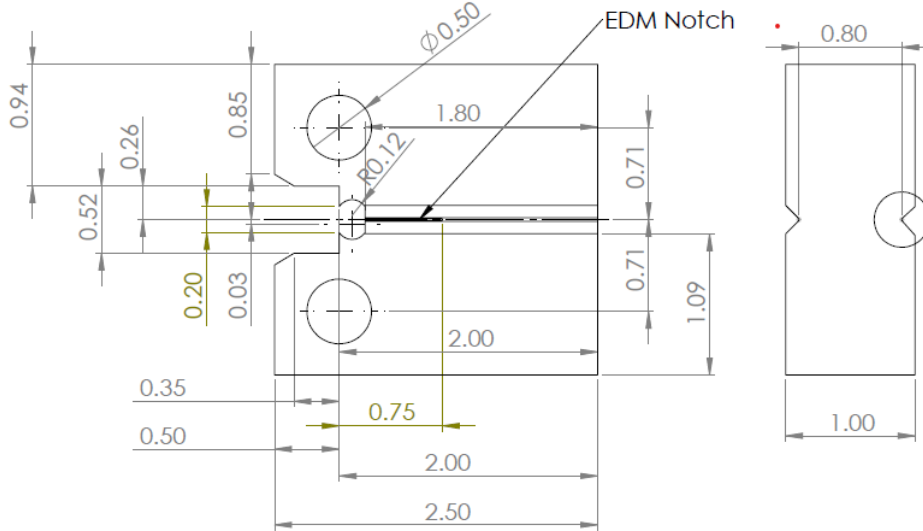


Figure B.2 Compact tension specimen geometry for baseline air fracture toughness

This document is not an API Standard; it is under consideration within an API technical committee but has not received all approvals required to become an API Standard. It shall not be reproduced or circulated or quoted, in whole or in part, outside of API committee activities except with the approval of the Chairman of the committee having jurisdiction and staff of the API Standards Dept. Copyright API. All rights reserved.

B.2 TEST METHODS

In this testing program, slow strain rate (SSR), fracture toughness (FT), permeation tests were performed. The SSR testing was performed on Alloy 718-120 only in 100-bar hydrogen and 100-bar helium (inert) environments. The FT testing was performed in air and 100-bar hydrogen gas on 4140-110 and Alloy 718-120. The permeation testing was performed on Alloy 718-120 only. High-purity hydrogen gas (99.999%) was utilized for all hydrogen testing. The following sections describe the test methods for the identified tests.

B.2.1 SSR Testing

SSR testing in 100-bar helium (inert) and 100-bar hydrogen gas environments was performed in accordance with ASTM G142. This testing utilized a servo-hydraulic test frame outfitted with an autoclave for high-pressure high-temperature hydrogen gas testing. Tests were controlled at a constant actuator displacement rate to achieve a target strain rate of $1 \times 10^{-5} \text{ s}^{-1}$, and test data were collected from each test with a LabVIEW-based data acquisition system. The gage section displacement was measured in-situ using an extensometer, and strain was calculated from this local displacement measurement. For each test, the load, pressure, extensometer, and actuator LVDT displacement were continuously collected. The autoclave preparation followed standard lab procedures for ensuring gas quality as previously described.

Stress-strain curves were developed for each test, and the following tensile test parameters were determined: 0.2% yield stress, the ultimate tensile stress, % elongation (both total, plastic), time to failure, % reduction in area (RA) etc. were determined. The elongation was determined from gage marks scribed on the specimen before testing, and after testing this distance was measured using a traveling microscope and compared to the initial distance. The reduction of area was calculated from the minimum diameter of each specimen after testing and the specimen diameter before testing. The inert (helium) test data were compared to the gaseous hydrogen data.

B.2.2 FT Testing

The objective of this task was to apply the test method E1820 to measure the crack initiation toughness (J or K_I) and cracking resistance curves (J-R curves) of each material in air and 100-bar hydrogen gas. Test specimens were fabricated per the cut plan and specimen drawings and then fatigue pre-cracked in lab air. After pre-cracking, specimens were side grooved to nominally 20% (10% each side). For the hydrogen gas tests, specimens were not pre-charged or presoaked, and testing was started as soon as steady-state conditions (temperature and pressure) were achieved in the autoclave. The crack initiation toughness and cracking resistance curves were measured on duplicate specimens for each material in 100-bar hydrogen gas. In addition to these hydrogen gas tests, test method E1820 was performed on at least one specimen for each material in lab ambient conditions to determine the baseline crack initiation toughness and J-R behavior.

This document is not an API Standard; it is under consideration within an API technical committee but has not received all approvals required to become an API Standard. It shall not be reproduced or circulated or quoted, in whole or in part, outside of API committee activities except with the approval of the Chairman of the committee having jurisdiction and staff of the API Standards Dept. Copyright API. All rights reserved.

The elastic-plastic fracture mechanics methods in ASTM E1820 were utilized to measure fracture initiation toughness and crack growth resistance. The anticipated fracture toughness values (J_{IC}) from the technical literature were used with the yield stress of each material to determine the minimum specimen thickness (B) and remaining ligament length determined by the specimen width and crack length (a) to ensure J-dominance and valid toughness results.

$$W - a, B > 10J_Q/\sigma_Y$$

Integral knife edges were fabricated into the specimens to measure the load-line crack opening displacement (COD) throughout each test. Integral knife edges allowed secure attachment of COD or clip gages to the test specimens. Following fabrication, the specimens were polished in and around the crack extension zone, and a lab data sheet was created to document test specimen dimensions and subsequent test steps. After pre-cracking and side-grooving, the hydrogen gas tests were instrumented with direct current potential drop (DCPD) probes to measure the in-situ crack extension.

The hydrogen gas tests were performed in autoclaves coupled to servo-hydraulic test frames. The test specimens were placed into the load train, and the DCPD wires were fed through ports in the autoclave head. The COD gage was attached, and DCPD probes were connected to the test system. The system was sealed, leak-checked using high-pressure nitrogen gas, and then purged using standard operating procedures. To ensure gas purity in the test autoclave, the autoclave was placed under vacuum, and a series of nitrogen gas and hydrogen gas purges were performed. The autoclave was then pressurized with high-purity hydrogen gas to the prescribed testing pressure. These procedures have been verified with gas sampling to achieve less than 1 ppm O₂ and less than 5 ppm H₂O. As prescribed in ASTM E1820, tests were performed under actuator displacement control at a constant rate. The displacement rate was calculated based on specimen dimensions and compliance to achieve a target initial K-rate of 1 MPa√m per hour (or 0.91 ksi√in. per hour).

For the air tests, the unloading compliance method was utilized to infer crack length from the specimen compliance by periodically unloading the specimens during the tests, and for the hydrogen gas tests, the crack length was measured using direct current potential drop (DCPD) as outlined in ASTM E1820 Annex 18 and periodic unloads were not used to infer crack length. The air tests were controlled and post-test analyzed using Fracture Technology Associates (FTA) software and hardware. This software automates the periodic unloading segments and accurately controls the test. The FTA software has an integrated software package for post-test analysis to develop J-R curves, identify the cracking initiation toughness (J_Q), and determine if validity requirements were satisfied.

For the hydrogen gas tests, load, crack-opening displacement, and DCPD voltage (converted to crack length) were continuously measured throughout each test using a LabVIEW-based data acquisition system. Based on these data, the J versus crack extension (Δa) curves were constructed using a MATLAB script following procedures specified in ASTM E1820. The crack length was calculated per a linear transformation from DCPD voltage and not as outlined in Annex 18 of the standard. From this construction, the crack initiation toughness (J_Q) was identified, and all validity criteria were evaluated.

B.2.3 Hydrogen Permeation Testing at High Pressure

Hydrogen permeation testing was performed in a specialized stainless-steel high-pressure autoclave test apparatus. Testing was performed using an electrochemical technique per ASTM G148. This assembly, which is shown in Figure B.5 has two chambers: a charging side with the high-pressure gaseous environment and an oxidation side where the hydrogen permeating through the sample is measured. The holder was fabricated to adjust the exposed area considering the strength of the material, thickness of the membrane and test pressure. The machined and Pd coated membrane was placed in the

This document is not an API Standard; it is under consideration within an API technical committee but has not received all approvals required to become an API Standard. It shall not be reproduced or circulated or quoted, in whole or in part, outside of API committee activities except with the approval of the Chairman of the committee having jurisdiction and staff of the API Standards Dept. Copyright API. All rights reserved.

holder in between two stainless steel plates. A seal is created by tightening the plates between the flanged ends. The charging side was then thoroughly deaerated and pressure checked prior to testing using 100% helium gas.

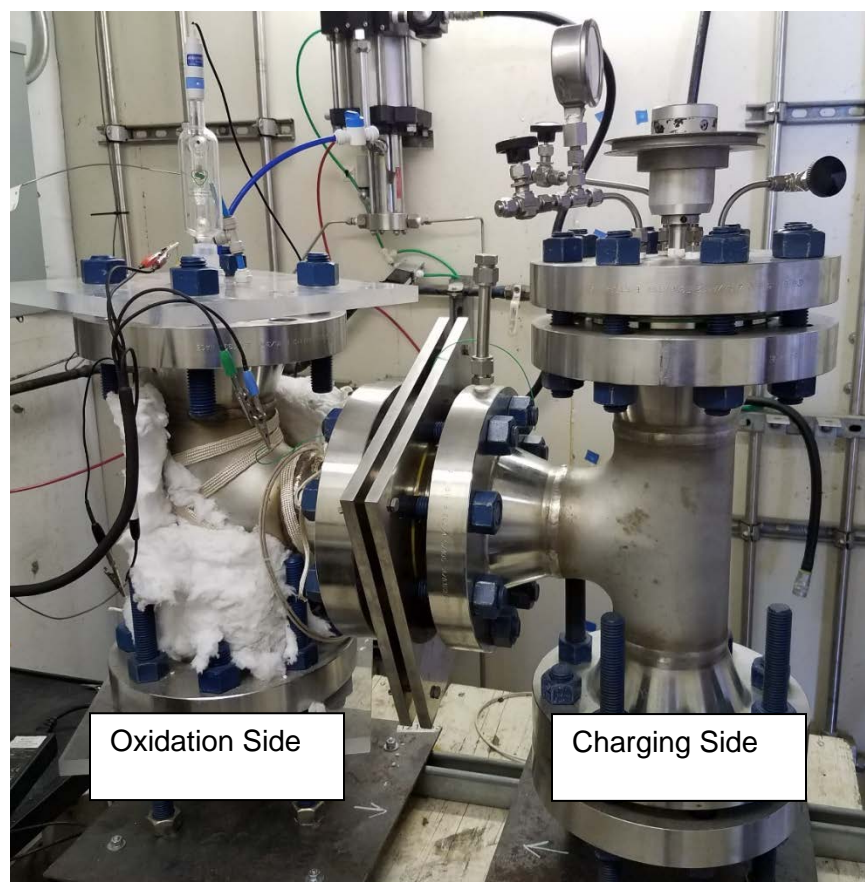


Figure B.5 High pressure permeation apparatus

A 0.1M NaOH solution was prepared separately and deaerated overnight using high purity Nitrogen gas. The solution was then transferred into the oxidation side of the test apparatus using the high purity Nitrogen gas to avoid oxygen inclusion. A platinum mesh was used as the counter electrode and Ag/AgCl electrode was used as the reference electrode. A +100 mV vs. SCE potential was applied on the sample and a background current was obtained in the nA range. It is beneficial to obtain a nA range background current to observe the current transient rise.

Once the background current was reached, a 100 bar (1,450 psi) H₂ gas was introduced into the charging side of the permeation cell at ambient temperature. During permeation testing, hydrogen diffuses through the membrane and becomes oxidized (on the oxidation side of the cell) and current is measured using a potentiostat. A current transient rise is then

This document is not an API Standard; it is under consideration within an API technical committee but has not received all approvals required to become an API Standard. It shall not be reproduced or circulated or quoted, in whole or in part, outside of API committee activities except with the approval of the Chairman of the committee having jurisdiction and staff of the API Standards Dept. Copyright API. All rights reserved.

observed and over time reaches a steady state (hydrogen permeation current). Measurements are recorded until a steady state current was obtained. The steady state hydrogen flux (J_{ss}) is obtained through the relationship:

$$J_{ss} = I / A * F$$

where,

I - steady state permeation current, Amp

A - area, cm²

F - Faradays constant, C/mol

Comment Only Ballot - For Committee Review